10

High-Voltage Insulators

10.1 Introduction

The basic role of high-voltage insulators is to ensure proper attachment of the line conductors to grounded support structures. In this respect, the insulators play two essential roles:

1. To ensure the electrical integrity of the system, under diverse weather conditions, by withstanding electrical stresses associated with system voltage as well as related temporary and switching overvoltages. While flashovers due to direct lightning strikes cannot be practically eliminated, these can certainly be managed down to acceptable levels.
2. To maintain the mechanical integrity of the system by withstanding mechanical stresses associated with conductor weight and related overstressing due to icing, wind load, broken conductor conditions, etc.

With the progressive increase of transmission line voltage from 33 to 1100 kV during the twentieth century, both the electrical stresses associated with the line voltage and the mechanical loads due to the massive conductor bundles represented a challenge to the insulator designer. It is obvious that EHV and UHV transmission lines with power transfer capacity of thousands of MW have to meet the highest standards of electrical and mechanical reliability. Such reliability has to be maintained over the prospective lifetime of the line, which designers take to be as long as 50 years or more. Present-day insulator designs have met this challenge satisfactorily. While the failure rate of individual glass or porcelain disc insulators may be typically 10^{-4} to 10^{-3} units per year, failures involving total mechanical collapse are very rare, in the order of 10^{-7} per year.

In the following, we will be reviewing the different materials and designs of high-voltage insulators, with special reference to high-voltage transmission lines. Specific sections deal with electrical and mechanical insulator performance, with due consideration to adverse weather conditions including the effects of rain and pollution. Insulator standards and testing are also addressed. Finally, both deterministic and statistical design approaches are discussed.

10.2 Insulator Types and Materials

10.2.1 Insulator Types

There are different basis to classify high-voltage insulators. On the basis of mechanical function, insulators can be classified into suspension or support insulators. Apart from medium-voltage lines where post insulators are used, suspension insulators on transmission towers prevail for high-voltage lines. On the other hand, insulator columns are widely used in high-voltage substations to carry tubular bus bars or other electrical equipment such as disconnecting switches or capacitor banks. Based on orientation, transmission line insulators can be classified into suspension strings in tangent or small-angle towers and tension strings in large-angle or terminal towers. For suspension strings, distinction could further be made between single or multiple I-strings or V-strings. The justification for applying

multiple I- or V-strings is normally based on mechanical or safety requirements, such as long spans associated with river or highway crossings.

Based on the profile of suspension insulators, distinction can be made among disc type and long-rod type, as shown in Figure 10.1 (Rizk et al., 1972), for a set of porcelain insulators. In Figure 10.1, three profiles A, B, and D show disc insulators, while C and E represent long rods. Figure 10.1(type A) shows a basically regular profile, while Figure 10.1(type D) represents a so-called antifog disc with deep ribs and long leakage path from the cap to the pin along the insulator surface. Figure 10.1(type B) shows a
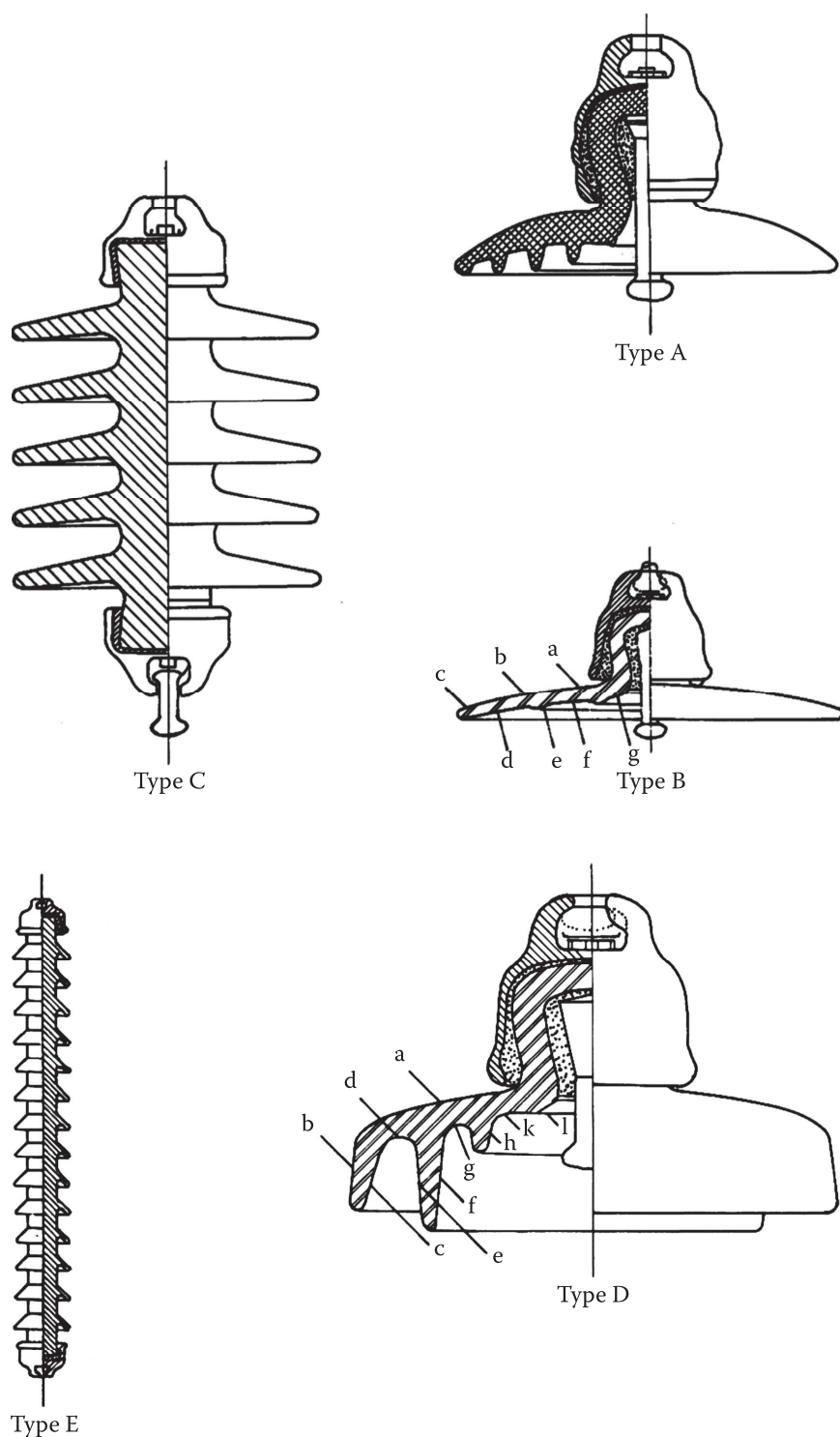

FIGURE 10.1   Profile of different cap and pin and long-rod porcelain insulators. (From Rizk, F.A.M. et al., Comparative tests on contaminated insulators with reference to desert conditions, CIGRE, Paper No. 33-03, 1972.)

TABLE 10.1

Basic Parameters of Insulators in Figure 10.1

Type	Leakage Path, mm	Spacing, mm	No. of Sheds	Outside Diameter, mm	Leakage Path/Spacing
A	384	183	—	320	2.10
B	419	178	—	483	2.54
C	1100	450	5	270	2.45
D	533	171	—	356	3.05
E	1850	1270	14	150	1.46

so-called aerodynamic disc, characterized by a relatively smooth profile and large overall diameter. Type E is a regular 75/14 long rod, while type C represents an aerodynamic long rod. Table 10.1 shows the basic parameters of the insulators shown in Figure 10.1.

In the following, we will return to the significance of these parameters and their effect on insulator performance, particularly under pollution conditions.

10.2.2 Insulator Materials

As far as insulator material is concerned, distinction should be made between ceramic insulators of porcelain and glass and polymeric or composite insulators. Material aspects are discussed in the following.

10.2.2.1 Porcelain

Electrical porcelain is made of a mixture of roughly 50% clay, 25% quartz or alumina, and 25% feldspar (Callister, 1994). Clays constitute some combination of hydrated aluminum silicate of one or more crystalline form, of a wide range of alumina (Al_2O_3) to silica (SiO_2) ratio. Quartz is chemically pure silica (SiO_2), while feldspar is a class of alkali–alumina–silicate minerals, for example, potash feldspar comprises $K_2O \cdot Al_2O_3 \, 6SiO_2$ (Young, 1954). The raw materials are mixed together and ground to the desired particle size. In the wet preparation process, these materials are mixed with water, and the resulting mixture is filtered to remove foreign particles. Actual forming is carried out by casting, extrusion, jiggering, and plunging (Young, 1954). For the dry preparation process, forming is performed by dry and vacuum pressing (Young, 1954). Forming is followed by drying, finishing, glazing, and firing, which is probably the most important operation in porcelain manufacturing (Young, 1954). It is obvious that the quality of porcelain depends not only on the raw materials but also on the skill of the manufacturer and on quality control.

Metal fittings are attached to porcelain by cementing. Fitting materials include malleable cast iron, ductile iron, and steel. The types of cement used include alumina cement, Portland cement and sulfur cement. Experience has shown that some problems could be encountered with sulfur cement in hot climates, while Portland cement could suffer in industrial environment that includes sulfates. Tables on physical properties of electrical porcelain are available in material science texts (Young, 1954; Callister, 1994) and in IEC 60672. Some properties are summarized in the following:

- Density: ≈ 2.5 g/cm^3.
- Tensile strength of porcelain depends on composition and varies in the range of 40–80 MPa.
- Compressive strength of porcelain is about an order of magnitude higher than its tensile strength.
- Volume resistivity is of the order of 10^{11} $\Omega \cdot$ m.
- Relative permittivity ε_r at room temperature and power frequency: 6–7.
- Dielectric strength is typically 200 kV/cm but depends on the thickness of the specimen.
- Maximum safe operating temperature is approximately 160°C.

- Coefficient of linear expansion $\approx 5 \times 10^{-6}$ (1/K).
- Thermal conductivity ≈ 1–4 W/m $\cdot$ K.
- Tan δ at power frequency: 1–3×10^{-2}.

The aforementioned properties lead to many advantages and some limitations of porcelain insulators (Vosloo et al., 2004). On the positive side, porcelain insulators are immune to degradation due to environmental factors, are resistant to surface damage due to leakage current, and have high compressive strength. They are, however, vulnerable to breakage and cracking due to power arcs and, when punctured, take specialized techniques (Vaillancourt and Rizk, 1988) to detect.

10.2.2.2 Glass

The soda lime glass consists of a melt of a mix of silica (SiO_2), limestone (CaO), feldspar ($Na_2O \cdot Al_2O_3 \cdot 6SiO_2$), and soda ash ($Na_2O$). Difference from porcelain arises primarily from its method of forming rather than from its ultimate composition (Young, 1954). In glass manufacturing, raw material mix is melted in a suitable furnace and then cooled to a lower temperature to become more viscous and can be worked into the desired shape. For cap and pin glass insulators, a heat treatment process called toughening is applied. This comprises reheating to a uniform temperature between transition and softening temperatures, followed by rapid quenching by exposing the surface to jets of cold air.

Relevant physical properties of toughened glass are summarized in the following:

- Density: ≈ 2.5 g/cm^3.
- Tensile strength is in the range of 100–120 MPa, somewhat higher than porcelain.
- Similar to porcelain, the compressive strength is considerably higher, reaching 700 MPa.
- Volume resistivity is similar to porcelain: $\approx 10^{11}$ $\Omega \cdot$ m.
- Relative permittivity at room temperature and power frequency: ≈ 7, close to porcelain.
- Dielectric strength somewhat higher than porcelain and, as other solids, decreases with sample thickness.
- Maximum operating temperature is somewhat lower than porcelain and could be as low as 110°C (Bartnikas, 1993).
- Coefficient of linear expansion: $\approx 9 \times 10^{-6}$, significantly higher than porcelain.
- Thermal conductivity: ≈ 1 W/m $\cdot$ K, significantly lower than porcelain.
- Tan δ at power frequency: up to 6×10^{-2}, significantly higher than porcelain.

The positive features of glass insulators (Vosloo et al., 2004) include high dielectric strength and resistance to puncture, easy detection of damaged insulators due to shattering, and good compressive strength. On the other hand, glass insulators constitute a target for vandalism and are susceptible to erosion due to leakage current, which can precipitate shattering. Cap and pin glass insulators assume similar shapes to porcelain discs shown in Figure 10.1.

10.2.2.3 Polymers

Polymeric insulators for high-voltage transmission lines comprise a resin-embedded fiberglass core, which provides mechanical strength and a polymeric cover for protection from adverse weather conditions. Two housing materials are presently in use: ethylene propylene diene monomer (EPDM) and silicone rubber. Silicone rubber is resistant to UV radiation and has hydrophobic property. This makes composite insulators with silicone rubber sheds a viable alternative to ceramic insulators in polluted regions. Silicone rubber is made from polydimethylsiloxane with the mer structure shown in Figure 10.2 (Young, 1954; Rosen, 1971; Callister, 2004), which, as elastomers, are cross-linked.
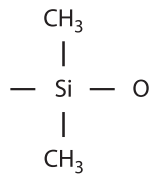
$$
\begin{array}{c}
CH_3 \\
| \\
-\ Si\ -\ O \\
| \\
CH_3
\end{array}
$$

FIGURE 10.2 Chemical structure of polydimethylsiloxane.

Some relevant physical properties of silicone rubber material are given in the following (Young, 1954; Rosen, 1971; Bartnikas, 1993; Callister, 2004; Vosloo et al., 2004):

- Density: ≈ 1.15 g/cm^3.
- Glass transition temperature T_g: $-120°C$. This means that the material retains its rubber behavior in very low temperatures.
- Maximum operating temperature: $\approx 350°C$.
- Relative permittivity at room temperature under power frequency: ≈ 4.
- Tan δ at room temperature under power frequency: 2–3×10^{-2}.
- Dielectric strength at power frequency: 160–200 kV/cm.
- Volume resistivity: 10^{12} Ω · m.
- Elongation to rupture: 150%–300%.

Note that these numbers, as those given for porcelain and glass earlier, are material properties. Accordingly, figures such as maximum operating temperature cannot obviously be applied to characterize an insulator unit, which results from application of different materials and manufacturing processes.

A typical design of a composite silicone rubber insulator (Dietz et al., 1986) is shown in Figure 10.3. It includes a fiber reinforced polymer (FRP) rod, which is chemically bonded to a high-temperature vulcanized (HTV) silicone rubber sheath. HTV silicone rubber sheds are vulcanized to the sheath. The FRP rod is attached to the end metal fittings by a cleaving wedge. The techniques used to attach the FRP rod to the end fittings include crimping, use of a cleaving wedge as in Figure 10.3, or application of an epoxy wedge within the end fitting.

It is important to ensure proper sealing between the end fitting and the silicone rubber sheath to avoid ingress of moisture. This and the chemical bond between the FRP rod and the sheath are intended to produce a puncture-free interface zone (Dietz et al., 1986). Typical dimensions of a silicone rubber composite
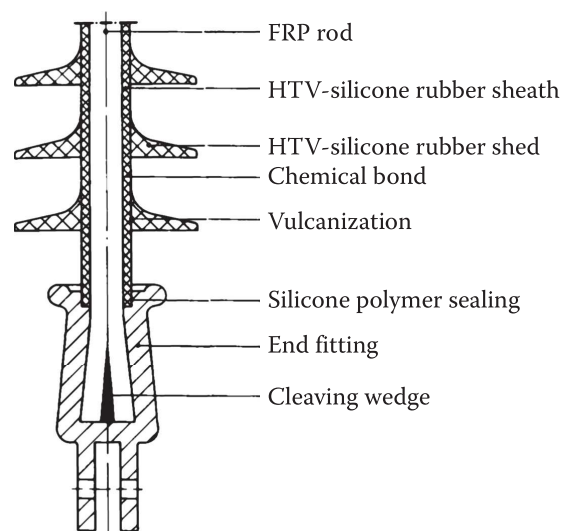

FRP rod
HTV-silicone rubber sheath
HTV-silicone rubber shed
Chemical bond
Vulcanization
Silicone polymer sealing
End fitting
Cleaving wedge

FIGURE 10.3 Typical details of a composite long-rod insulator. (From Dietz, H. et al., Latest developments and experience with composite long-rod insulators, CIGRE, Paper No. 15-09, 1986.)
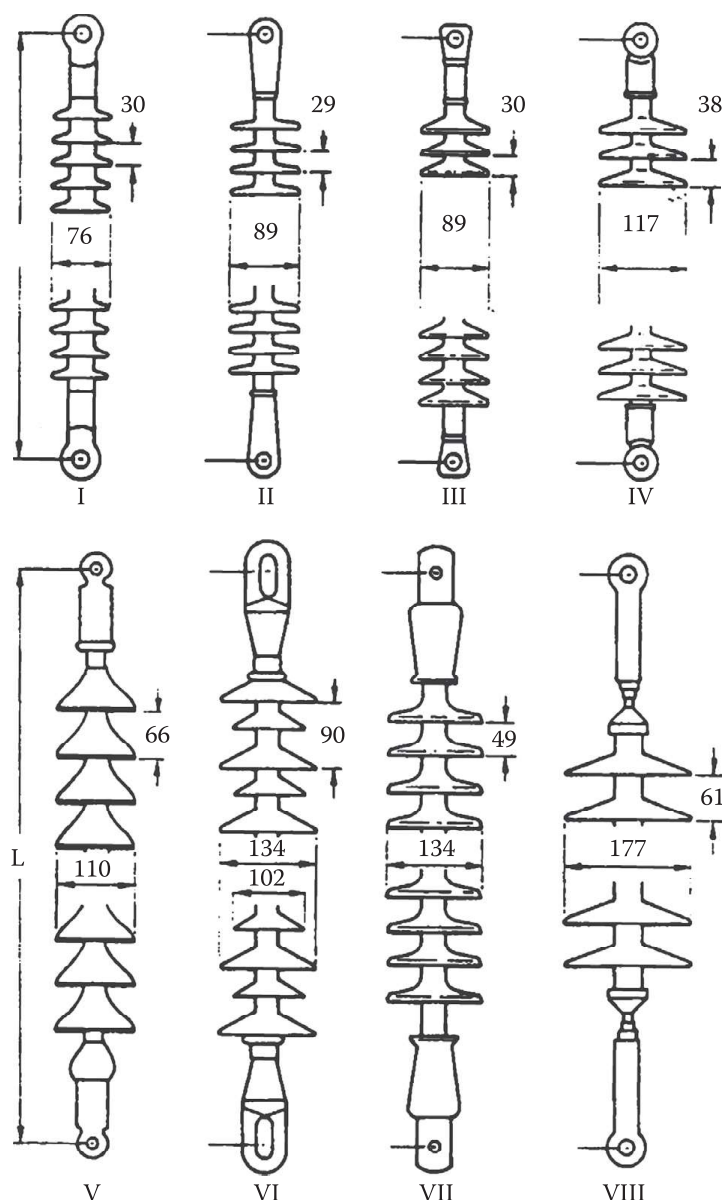
FIGURE 10.4 Profile of different nonceramic insulators. (From Houlgate and Swift, 1990.)

insulator are shown in Figure 10.4 (Houlgate and Smith, 1990). For type VII insulator, the shed spacing is 49 mm, outside diameter 134 mm, length L of 2.46 m, and leakage path length L_c 5.93 m. Using such insulator unit at a system voltage U_m of 245 kV results in a specific leakage path $l_{sp} = L_c/U_m$ of 24 mm/kV.

For system voltages of 245 kV and above, it is often recommended to provide polymeric insulators with protective rings. Such rings serve different purposes, including RI control, protection of end fittings from power arcs, as well as inhibiting housing material erosion due to surface discharge activity (Cherney et al., 1983; Phillips et al., 1999). Definitions, test methods, and acceptance criteria for composite insulators are given in IEC Standard 61109 (1992).

10.3 Electrical Performance of High-Voltage Insulators

10.3.1 Lightning Impulse Flashover

As mentioned in the chapter on long air gaps, lightning impulse sparkover takes place according to a streamer breakdown mechanism, since impulse duration is too short to allow any significant leader growth. Lightning impulse flashover of insulator strings is effectively a streamer breakdown of the air

gap between the conductor and the cross arm or between the guard rings or along the string arcing distance, whichever is shorter.

For strings of 2–6 standard cap and pin discs, Figure 10.5 (Rizk, 1960) shows a linear relationship between the number of insulator units and lightning impulse flashover voltage. As shown, negative impulse flashover voltage is only about 5% higher than with positive polarity. Figure 10.6 (Paris and Cortina, 1968) shows positive and negative standard lightning impulse flashover voltage of an insulator string, with conductor crossarm gap in the range of 2–6 m. Again, a linear relationship is shown with
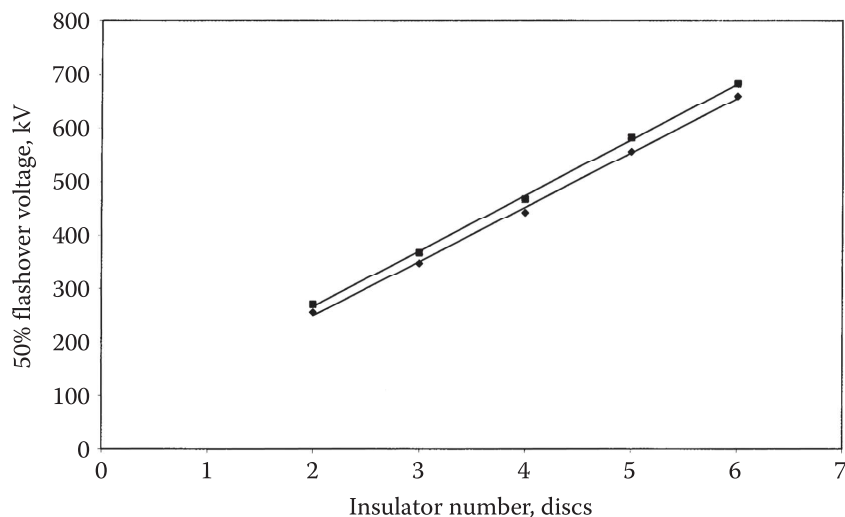

FIGURE 10.5 Standard lightning impulse flashover characteristics of short insulator strings. Upper: negative; lower: positive. (From Rizk, F.A.M., Flashover characteristics of insulators and spark-gaps with a power frequency half-cycle pulse, Thesis, Royal Institute of Technology, Stockholm, Sweden, 1960.)
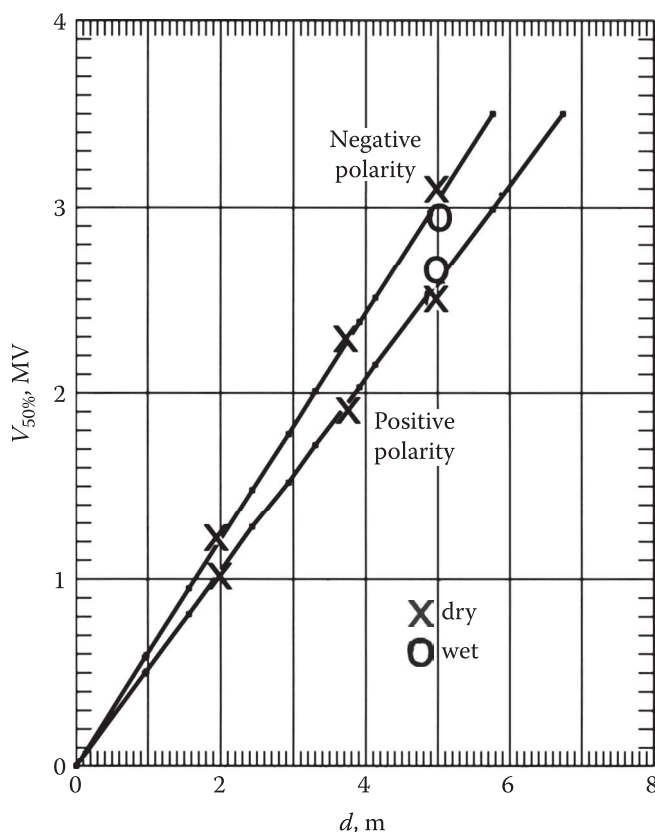

FIGURE 10.6 Lightning impulse flashover characteristics of dry and wet insulator strings. (From Paris, L. and Cortina, R., *IEEE Trans. Power Appar. Syst.*, 87(4), 947, April 1968.)

the negative impulse flashover voltage slightly higher than the positive. The mean positive breakdown gradient amounts to approximately 525 kV/m, while the negative is approximately 600 kV/m. Note that these numbers would be affected by design and positioning of guard rings.

It is also noted in Figure 10.6 that the flashover results of dry and wet insulator strings under standard lightning impulse practically coincide. This confirms that rain has practically no effect on lightning impulse flashover. In fact, international standards do not require a lightning impulse wet test on insulator strings (IEC Standard 60305, 1995).

Lightning impulse flashover of transmission line insulators can influence lightning performance of the line in two ways. First, as mentioned in Chapter 9 on lightning, the minimum stroke current that can lead to flashover following a shielding failure is given by:

$$I_c = \frac{2U_b}{Z_0} \tag{10.1}$$

where

U_b is the negative lightning impulse flashover voltage of the line insulation
Z_0 is the line surge impedance

Since, as explained previously, there is a maximum current I_m at which shielding failure can occur, increasing I_c by reinforcing line insulation will result in reducing SFFOR.

Ultimately, if $I_c = I_m$, SFFOR will vanish. It is an economic question, whether it would be more advantageous to reduce I_m by proper positioning of the overhead ground wire, or increase I_c by reinforcing line insulation.

The second aspect, also treated in the Chapter 9 on lightning, is the effect of line insulation of backflashover. Here, the critical current level I_{cb} for backflashover was expressed by (Hileman, 1999)

$$I_{cb} = \frac{V_{NS} - K_{PF}V_{LN}}{(1 - C)K_{TT}} \tag{10.2}$$

where

V_{NS} is the critical nonstandard lightning impulse flashover voltage of the insulator string
V_{LN} is the phase-to-ground power frequency voltage
K_{PF} is the power frequency voltage factor
K_{TT} is the tower top potential coefficient
C is the coupling factor between the phase conductor and ground wire

It is clear from (10.2) that reinforcing line insulation will increase V_{NS} and accordingly I_{cb}. Under otherwise the same conditions of tower design and tower grounding, it is obvious that reinforcing of line insulation will then lead to reduction of the backflashover rate.

An illustrative simplified example is shown in Figure 10.7, based on Monteith et al. (1964), which presents variation of the backflashover rate per 100 km · year with the tower footing resistance of a 138 kV line, with 8, 10, and 12 insulators. Here, the span is 275 m and the keraunic level is 30. The backflashover rate is sensitive to both the footing resistance and the number of insulator discs. Again, the choice in order to satisfy the line performance criterion is economic. If it is required, for example, to limit the backflashover rate to 1.0/100 km · year, then with a 10 Ω footing resistance an 8-disc string will be adequate. For a 20 Ω footing resistance, on the other hand, the performance criterion can only be met with a 12-disc string. In this example, the insulator-specific leakage path amounted to 17, 21, and 26 mm/kV for 8, 10, and 12 discs, respectively. As will be shown later in this chapter, the line insulation is often dictated by insulator pollution requirements. In such situations, it may be found that the backflashover performance criterion is met even for nonrestrictive values of the tower footing resistance.

Finally, another effect of the lightning impulse flashover characteristics of line insulation is that it sets the upper limit for the amplitude of impinging impulses into the substation (Hileman, 1999).
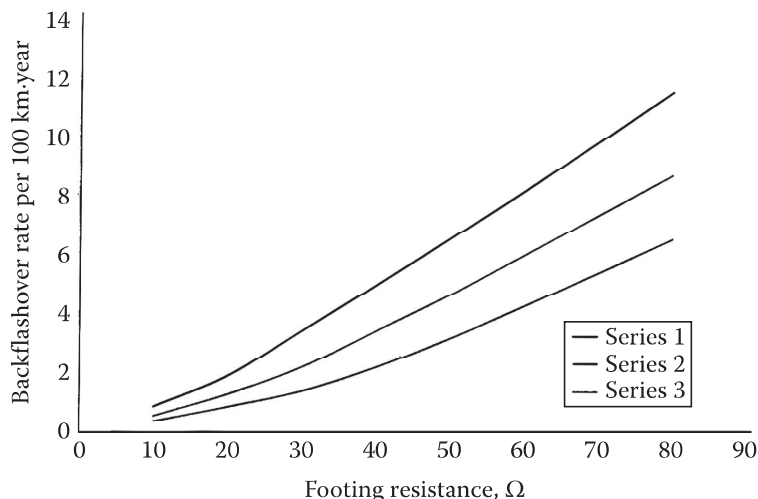
FIGURE 10.7 Variation of backflashover rate with tower footing resistance for different numbers of disc insulators in a 138 kV line. Span: 275 m; keraunic level: 30. S1: 8 insulators; S2: 10 insulators; S3: 12 insulators. (From Monteith, A.C. et al., Line design based upon direct strokes, in: *Electrical Transmission and Distribution Reference Book*, Westinghouse Electric Corporation, East Pittsburg, PA, 1964, pp. 578–609, Chapter 17.)

TABLE 10.2

Effect of Insulator String on Switching Impulse Flashover of a Conductor: Tower Crossarm Gap

	U_{50}, kV	
Applied Impulse	**Gap without Insulators**	**19-Disc String**
Positive switching	1160	1132
Negative switching	1478	1449

Source: LeRoy, G. et al., *Les propriétés diélectriques de l'air et les très hautes tensions*, Eyrolles, Paris, France, 1984, Chapter 16.

10.3.2 Switching Impulse Flashover

10.3.2.1 Comparison with Air Gaps

Here again, switching impulse flashover of an insulator string under dry conditions is basically a breakdown of the corresponding air gap. This occurs with the stages explained earlier of critical streamer formation, continuous leader inception and propagation, and final jump. Table 10.2 extracted from LeRoy et al. (1984) shows that there is little difference between the switching impulse strength of an insulator string, here consisting of 19 cap and pin discs, and the corresponding air gap without insulators.

10.3.2.2 Effect of Rain

An extensive experimental study on the effect of rain on switching impulse flashover of both insulator strings and supporting porcelain columns is reported in Rizk (1975). It was found that for positive polarity, the discharge path is displaced away from the insulator position (Figure 10.8). This explains the finding that positive switching impulse flashover voltage of both insulator strings and supporting columns is rather insensitive to rain intensity and resistivity within the ranges investigated. On the other hand, negative switching impulse discharge path takes place in proximity of the insulator and, accordingly, is more sensitive to rain parameters.

These points are illustrated in Figure 10.9 (Rizk, 1975). It is shown that, for a 25-disc insulator string, the positive switching impulse flashover voltage, apart from statistical scatter, is independent of the rain resistivity. Negative switching impulse flashover voltage, however, increases slightly with the increase of
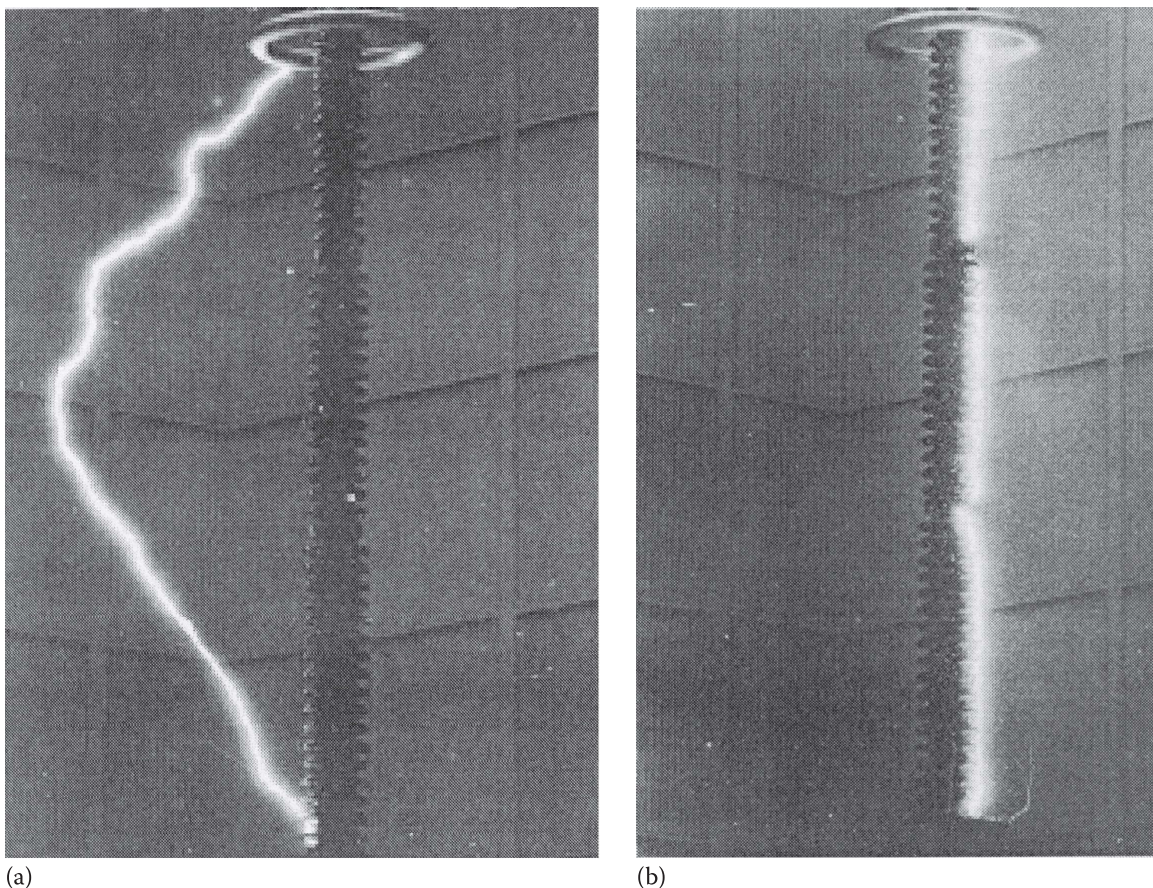
FIGURE 10.8 Typical switching impulse flashover path on an insulator column. (a) Positive polarity and (b) negative polarity. (From Rizk, F.A.M., *Proc. IEE*, 122(4), 449, April 1975.)
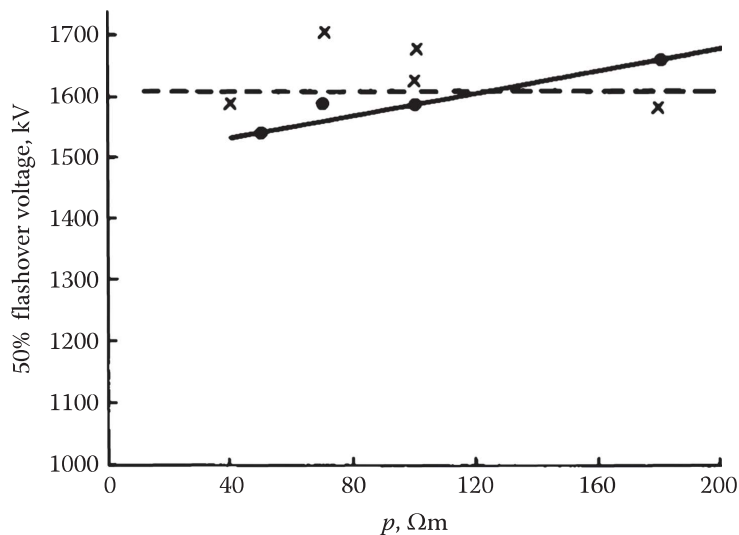

FIGURE 10.9 Variation of wet switching impulse flashover voltage of a disc string with water resistivity. x—Positive and *—negative. (From Rizk, F.A.M., *Proc. IEE*, 122(4), 449, April 1975.)

rain resistivity. The same trend is confirmed in Table 10.3 (Rizk, 1975), which presents the ratio of wet to dry switching impulse flashover voltage for a 25-disc string.

Similar results are presented in Table 10.4 for a 4.7 m supporting porcelain insulator column. Here again, there is practically no effect of rain on positive switching impulse flashover voltage, while there is a significant decrease for negative polarity. Finally, it should be mentioned that, in general, high-voltage rain tests are notorious for their relatively large dispersion, particularly for short wetting time (Figures 10.10 and 10.11) (Rizk and Hyltén-Cavallius, 1974).

TABLE 10.3

Effect of Rain of 50% Flashover Voltage of a 25-Disc String on Polarity of Switching Impulse

Applied Impulse	Rain Parameters Intensity, mm/min	Resistivity, Ω · m	Wet FOV, % Dry FOV
Positive switching	5	100	103
Negative switching	5	100	87

Source: Rizk, F.A.M., *Proc. IEE*, 122(4), 449, April 1975.

TABLE 10.4

Effect of Rain on Switching Impulse Flashover of 4.7 m Insulator Column

Test Condition	Rain Parameters Intensity, mm/min	Resistivity, Ω · m	U_{50}, kV Positive	U_{50}, kV Negative
Dry	—	—	1654	>2400
Wet	5	100	1637	1855

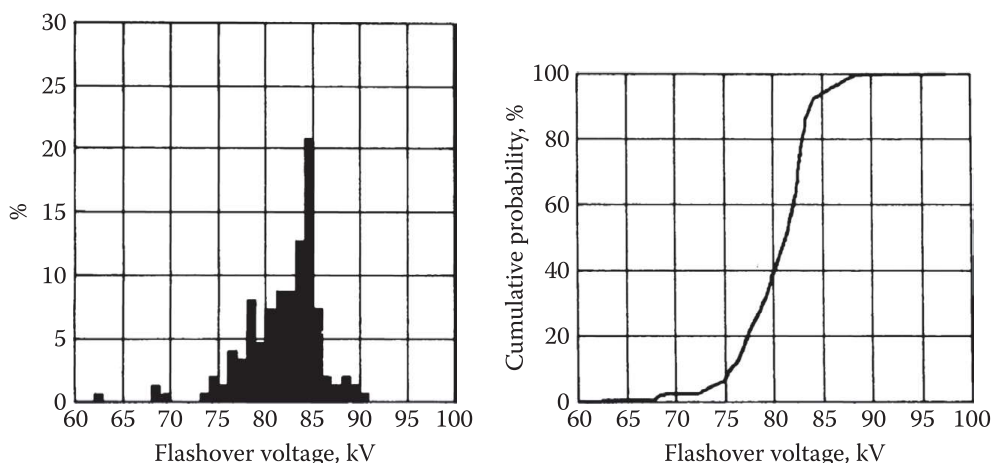*Source:* Rizk, F.A.M., *Proc. IEE*, 122(4), 449, April 1975.

FIGURE 10.10 Frequency histogram and cumulative distribution curve of wet switching impulse flashover of a standard disc insulator. Wetting time: 0–18 min. (From Rizk, F.A.M. and N. Hyltén-Cavallius, Wetting of high-voltage insulators by artificial rain, IEEE Conference Paper C74 074-1, Winter Power Meeting, New York, 1974.)

FIGURE 10.11 Frequency histogram and cumulative distribution curve of wet switching impulse flashover of a standard disc insulator. Wetting time: 18–45 min. (From Rizk, F.A.M. and N. Hyltén-Cavallius, Wetting of high-voltage insulators by artificial rain, IEEE Conference Paper C74 074-1, Winter Power Meeting, New York, 1974.)
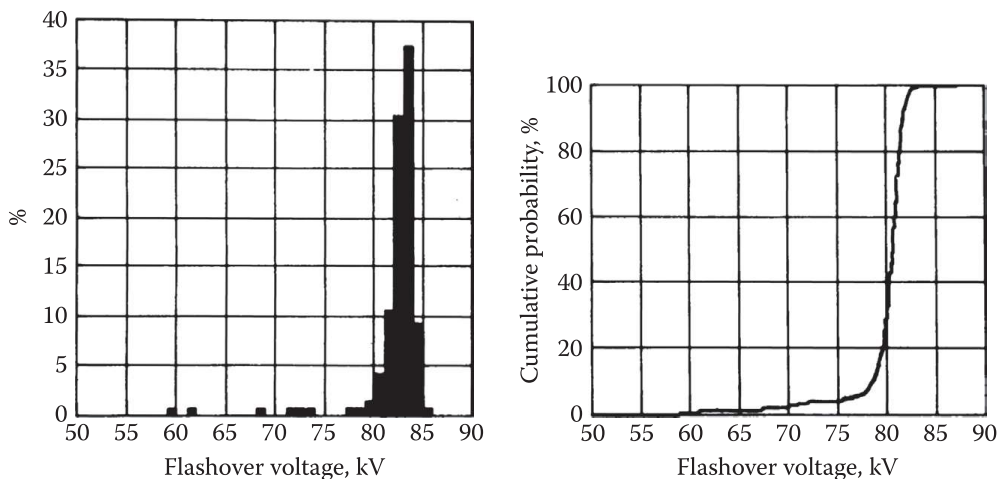
10.3.3 Pollution Flashover

Flashover of insulators under system operating voltage has been experienced in heavily polluted industrial environment, near the seacoast, and in the desert. It is now recognized that pollution flashover mechanism is characterized by different stages: contamination layer buildup, insulator wetting, leakage current surging, formation of dry-band arcs, and eventual extension of such arcs to span the whole leakage path. In this chapter, such stages are dealt with and pollution flashover characteristics of insulators of different materials and designs are presented. High-voltage laboratory testing of polluted insulators is also included.

10.3.3.1 Pollution Layer Buildup

A pollution layer is formed when airborne particles settle on the insulator surface. The forces governing the motion of airborne particles involve wind forces, gravitational forces, and forces due to the electric field distribution in the insulator vicinity (Witt, 1961). The resultant force **F** is the vector sum of these forces. It may be instructive to look at these individual forces.

As we are dealing with fog and dust particle sizes in the range of 10–100 μm (Humphreys, 1964; Rizk et al., 1975), motion under gravity will be governed by Stoke's equation (Rouse, 1961; Kikoin and Kikoin, 1978). For a spherical particle of radius r and density ρ, the terminal speed v_t is reached when the viscous frictional force is equated to the gravitational force:

$$6\rho r h v_t = \frac{4}{3}\rho r^3 (r - r_a) \lozenge g \tag{10.3}$$

where

ρ_a is the air density
η is the viscosity of air
g is the gravitational constant, 9.81 m/s²

This yields the following expression for the terminal velocity v_t:

$$v_t = \frac{2}{9} g r^2 \frac{(r - r_a)}{h} \tag{10.4}$$

Using (10.4) with $\rho_a = 1.29$ kg/m³ and $\eta = 1.72 \times 10^{-5}$ kg/m · s, Table 10.5 gives estimates, for $10 \le r \le 80$ μm, of v_t, for both dust particles of different dimensions and for fog.

It is shown that for most particle sizes in the earlier range, the terminal velocity under gravity is much lower than any practical wind speed.

Under wind conditions, with a wind speed v_w, motion of particles in the earlier size range can also be described by Stoke's equation. For a spherical particle of radius r, the wind force F_w can be expressed as

$$F_w = 6\rho r h (v_w - v) \tag{10.5}$$

where v is the particle speed at any instant, in the direction of v_w.

TABLE 10.5

Calculated Terminal Velocity under Gravity of Different Airborne Particles

Particle	Diameter, μm	Density ρ, kg/m³	Velocity v_t, m/s
	10	1500	0.0048
	20		0.019
Dust	40		0.076
	60		0.171
	80		0.304
Fog	10	1000	0.003

Only for $v = 0$ would $F_w \rightarrow 6\pi r \eta v_w$, while F_w would vanish if $v \rightarrow v_w$, since then there would be no viscous frictional force applied to the particle.

The acceleration of the particle exposed to wind could be obtained from (10.5) as

$$\frac{dv}{dt} = \frac{9}{2}\frac{\eta}{r^2 \rho}\left(v_w - v\right) \tag{10.6}$$

When integrated, this equation shows that $v \rightarrow v_w$ with a time constant $\tau = (2r^2\rho)/9\eta$. For a dust particle with a 50 μm diameter and $\rho = 1500$ kg/m^3, τ is determined at 12 ms. As expected, it does not take long before the particle assumes the wind speed v_w and there will be no more acceleration.

The present analysis for gravitational and wind forces on 10–100 μm particles and resulting accelerations differs from the approach described in Witt (1961).

The first electrical force $\mathbf{F}_{e1}$ acts on particles charged by corona in the insulator vicinity:

$$\mathbf{F}_{e1} = q\,E \tag{10.7}$$

where
    q is the particle charge
    E is the electric field at any point

The second is the dielectrophoretic force $\mathbf{F}_{e2}$ due to polarization of dust particles. Such force also depends on the particle shape and, for a spherical particle of radius r, can be expressed as

$$\mathbf{F}_{e2} = 2\pi r^3 \varepsilon_0 \frac{\varepsilon_r - 1}{\varepsilon_r + 2}\,\mathrm{grad}\left|E\right|^2 \tag{10.8}$$

where ε_r is the relative permittivity of the particle and

$$\left|E\right|^2 = E_x^2 + E_y^2 + E_z^2 \tag{10.9}$$

where E_x, E_y, and E_z are the x, y, and z components of the electric field at any point.

It is interesting to note that the force $\mathbf{F}_{e1}$ that acts on charged particles tends to drive the particles to zones of lower electric field. On the other hand, the dielectrophoretic force $\mathbf{F}_{e2}$ tends to drive the particles to zones of high electric field (Witt, 1961). It should also be noted that the force $\mathbf{F}_{e1}$ on charged particles may be relevant only under direct voltages, while the dielectrophoretic force $\mathbf{F}_{e2}$ applies for both ac and dc.

It should be noted that the pollution layer on the insulator surface is the result of complex interaction between the insulator shape and material and prevailing atmospheric conditions. In this respect, the site severity (CIGRE 33.04, 1979) does not become an abstract term characterizing the site alone but must account for the aforementioned interaction. This will be addressed in the following.

10.3.3.2 Site Severity

We should perhaps start with definition of equivalent salt deposit density (ESDD), which is often used to characterize pollution severity. The ESDD is the equivalent surface density of sodium chloride NaCl/cm^2, measured in mg/cm^2, which, when subjected to the same wetting, will produce the same surface conductivity χ_s in μS as the actual pollution layer. The procedure to measure ESDD is described in IEC 60507 (IEC Standard 60507, 1991). Another term used is the NSDD, which is the nonconducting surface deposit density, also measured in mg/cm^2. While nonconducting by itself, NSDD contributes indirectly to actual surface conductivity through its ability to absorb water. This will also influence drying of the pollution layer through leakage current surging as well as washing the layer off when exposed to prolonged wetting.

Methods used to assess site pollution severity include the following (CIGRE 33.04, 1979):

- Measurement of ESDD on different insulator types and design after certain exposure periods.
- Monitoring of the surface conductance of a sample insulator. The applied voltage level and duration have to be such as to avoid dry-band formation.
- Counting of leakage current surges exceeding a certain preset level.
- Recording to the highest leakage current I_h on a certain insulator, which does not lead to flashover (Verma, 1973).
- Measurement of the maximum current level I_{max} attained just before flashover (Verma, 1973).
- Measurement of the flashover stress, which is defined as the power frequency flashover voltage divided by the overall insulator length.
- Use of directional dust deposit gauges is described in Vosloo et al. (2004). This method does not account for the interaction between the insulator and the environment and will not be treated here further.

10.3.3.3 Effect of Exposure Time

As mentioned earlier, pollution layer buildup is a result of a complex interaction between the insulator and the environment. Pollution layer pattern is discussed in the following texts. An obvious factor influencing pollution layer buildup is the time of exposure. Also, self-cleaning due to wind and rain usually sets an upper limit for pollution severity but also depends on insulator shape. Open aerodynamic profiles have better self-cleaning quality than long leakage path profiles with deep under ribs. Also, frequency and intensity of dew formation influence layer buildup.

The rate of pollution accumulation, even for the same insulator design, clearly depends on location as shown in Figure 10.12 (Rizk et al., 1975). This refers to field tests on a 500 kV transmission of 800 km length in desert environment. The line is divided in four sections, each of which was considered to repre-
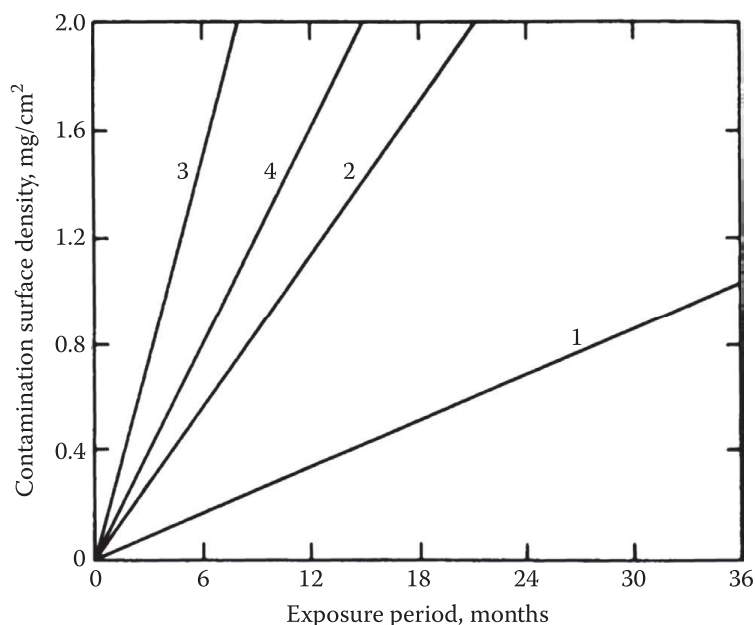

FIGURE 10.12 Contamination layer buildup on insulator surface with exposure period in the desert for different line sections. (From Rizk, F.A.M. et al., *IEEE Trans. Power Appar. Syst.*, 94(5), 1170, September/October 1975.)

sent distinct environmental conditions. The straight lines in Figure 10.12 represent the best fit of highly dispersed material. Several observations can be made:

- Different line sections have distinct rates of pollution accumulation.
- While section 3 reaches 2 mg/cm² of deposit (conducting and nonconducting) in 6 months, section 1 has apparently not reached saturation after 36 months of exposure. This is rather unfortunate since it necessitates long exposure periods during field tests in order to reach realistic severity levels for line design.

Chemical analysis of this natural contaminant showed that soluble salts amount to 18% by weight, mostly consisting of sulfates and chlorides: $CaSO_4 \sim 10\%$, $NaCl \sim 3\%$, and $KCl \sim 0.5\%$. This means that for section 3 of the line, a total deposit of 2 mg/cm², reached in 6 months of exposure, corresponds to 0.36 mg/cm² of soluble salt, which is extremely severe. This high content of soluble salts in the natural contaminant was quite surprising, since analysis of salt content from sand samples taken along the line route varied in the range of 1%–4%. This discrepancy was explained when grain size analysis of the contaminant and the soil samples were undertaken.

It was established that 95% by weight of the natural contaminant comprise a grain size less than 44 μm, and all grains were below 74 μm. Figure 10.13 shows variation of soluble salt content as a function of grain size in soil samples from the desert sand. It is observed that, for grain size above 100 μm, salt content is relatively small. On the other hand, for the small grains of the size found on the insulator surface, the salt content was excessive. It was then visualized that a grain selection process occurs on the insulator surface, whereby small grains stick while large grains are blown away by wind. Dew formation is likely to play an important role in this process.

It should be noted that the gradual buildup of pollution layer on insulator surface presented in Figure 10.12 does not apply to all regions. For example, stormy conditions from the sea, like typhoons in Japan, dump large amounts of salty water on the insulators in a matter of hours (Higashimori et al., 1995). Even in the desert, sandstorms dump large amounts of dry contaminants on transmission line insulators in a single day. In case of storms near the seashore, the phases of contamination buildup and insulator surface wetting are combined and, therefore, represent a serious hazard. As to sandstorms, the hazard depends on whether the sandstorm is quickly followed by drizzle. If no insulator surface wetting follows, however, the dry sand due to the storm is gradually blown away by wind with no serious consequences.
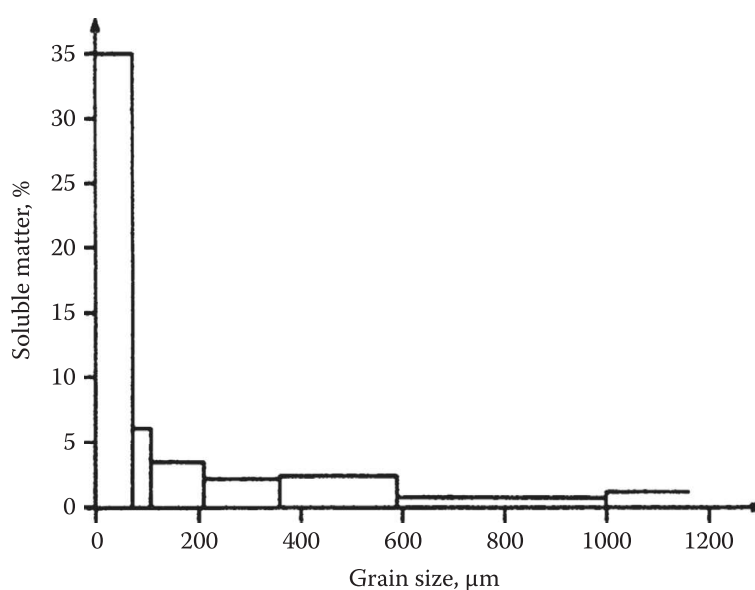

FIGURE 10.13 Variation of soluble salt content with grain size of a solid sample in the desert. (From Rizk, F.A.M. et al., *IEEE Trans. Power Appar. Syst.*, 94(5), 1170, September/October 1975.)

10.3.3.4 Pollution Layer Pattern

It has often been reported that for ceramic cap and pin insulators, the contamination surface density on the bottom ribbed surface can be as high as 5–10 times that of the upper surface (Rizk et al., 1975). The value depends of course on insulator profile and on the prevailing self-cleaning effect. Figure 10.14 (Rizk et al., 1975) shows the distribution of ESDD along the leakage path of antifog disc type D of Figure 10.1 after 24 months of exposure in desert environment, confirming the extremely high pollution captured in the deepest groove, points *c*, *d*, and *e*. The following groove, point *g*, was clearly protected by the first rib.

Figure 10.15 (Rizk et al., 1975) shows the corresponding ESDD distribution along the leakage path of the aerodynamic profile of insulator B of Figure 10.1. There is still extremely high pollution in the part *d–e–f* of the bottom surface. It is clear, however, that by integration over the surface, the total amount of pollution collected by the aerodynamic profile will be much lower than the antifog profile.

Pollution buildup on silicone rubber insulators has not been as extensively studied as on ceramic insulators. It has been reported (Higashimori et al., 1995) that marine-type pollution forms in isolated spots on the surface of a new silicone rubber insulator. However, with aging, as hydrophobicity is lost, the pollution layer becomes more uniform. For inland, it was reported that dust is deposited evenly on the polymeric insulator surface (Karady et al., 1995).
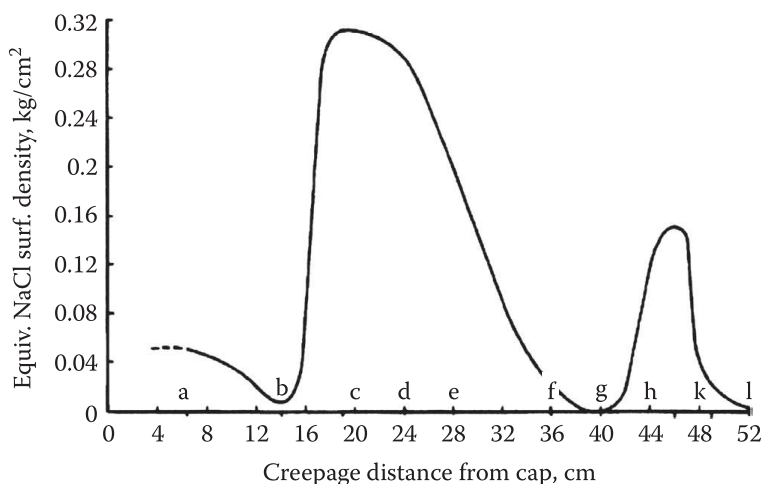

FIGURE 10.14   Distribution of ESDD along a path on the surface of an antifog disc—type D. (From Rizk, F.A.M. et al., *IEEE Trans. Power Appar. Syst.*, 94(5), 1170, September/October 1975.)
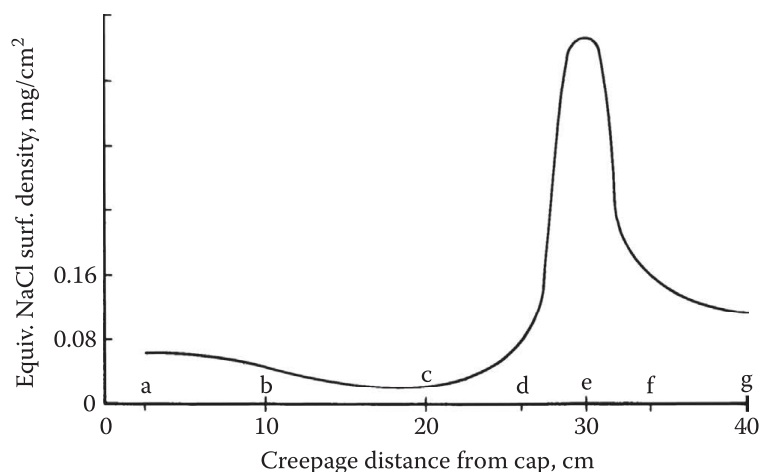

FIGURE 10.15   Distribution of ESDD on the surface of aerodynamic type B insulator. Cap: point a; pin: point g. (From Rizk, F.A.M. et al., *IEEE Trans. Power Appar. Syst.*, 94(5), 1170, September/October 1975.)

10.3.3.5 Effect of Operating Voltage

As previously mentioned in Section 10.3.3.1, the operating voltage effect on pollution layer buildup will manifest itself in the electric force $\mathbf{F}_{e1}$ exerted on charged particles and the dielectrophoretic force $\mathbf{F}_{e2}$. Estimates in Hall and Mauldin (1981) show that the force $\mathbf{F}_{e2}$ is small compared to gravitational and wind forces even for the not particularly high wind speed of 0.8 m/s (2.9 km/h). This is in agreement with long-standing field experience, which shows that, for ac lines, the operating voltage has little influence on pollution layer buildup. This in turn led to building of exposure tests stands sometimes with unenergized insulators to collect pollution deposit data for ac transmission line design (Akbar et al., 1995).

On the other hand, the effect of the force $\mathbf{F}_e$ on charged particles, associated with dc energization, is more complex. This effect can be assessed by comparison of severity with dc and ac energization. Such review was undertaken by Schneider (1993) and presented in Figure 10.16. It is shown that for moderately polluted zones, with ESDD $\sim$ 0.01 mg/cm^2, dc energization could lead to intensification of pollution layer buildup by a factor of 8. For zones with extremely high severity, for example, of ESDD $>$ 0.1 mg/cm^2 on the other hand, dc energization has practically no effect on layer buildup. This can be interpreted that for low pollution severity zones, the wind and gravitational effects are relatively small, which makes the effect of particle charging very significant. On the other hand, where wind and gravitational forces are large, dumping excessive pollution deposit on the insulator, the relative value of $\mathbf{F}_e$, becomes insignificant.

10.3.3.6 Effect of Distance from Pollution Source

Experience has shown that transmission line insulators in the vicinity of the seacoast may be exposed to severe marine pollution (Houlgate et al., 1982). However, this appears to be dependent on the direction of the prevailing wind. If the prevailing wind is from the sea into the land, the situation is most severe near the seacoast but improves with distance as we move inland.

Figure 10.17 shows the relationship between ESDD on standard porcelain disc insulators and distance from the seacoast, as reported from a Japanese investigation (Kimoto et al., 1972). There is substantial scatter in the ESDD results, but the definite trend is for reduction of severity with longer distance from the coast. It appears from Figure 10.17 that it takes a distance of about 50 km from the coast for the ESDD to stabilize to the inland level. This pollution buildup was attributed to calm wind, meaning that it was not caused by typhoons, but unfortunately the wind speed range involved was not reported (Kimoto et al., 1972). From the analysis of forces acting on airborne deposit particles given in Section 10.3.3.1, it is clear
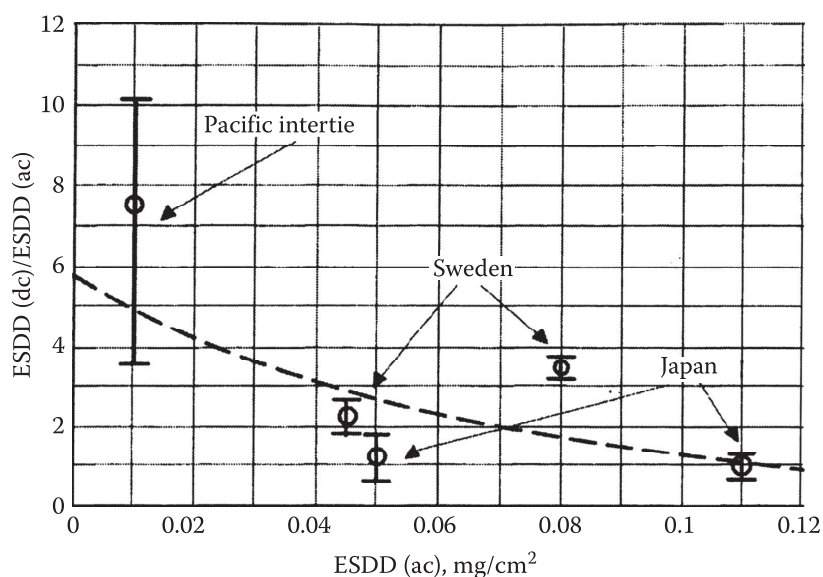

FIGURE 10.16 Ratio of ESDD collected on insulators energized with dc to that collected on ac—energized insulators. (From Schneider, H.M., *Insulation for HVDC Transmission Lines*. EPRI HVDC Reference Book, Chapter 5, September 1993.)
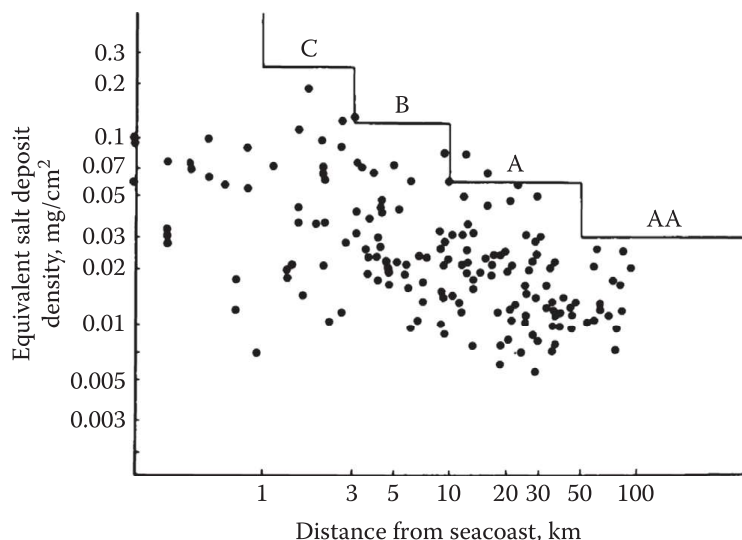
FIGURE 10.17 Variation of ESDD on insulators with distance from the seacoast. (From Kimoto, I. et al., *IEEE Trans. Power Appar. Syst.*, 91, 317, January 1972.)

that the distance affected by proximity to the seacoast will depend on wind speed and also on the particle size. Such distance will generally increase; the higher the wind speed, and the smaller the size of the pollutants. In this respect, salt fog particles will travel longer distance from the sea than heavier dust particles characterizing, for example, a combined marine and desert condition since the terminal gravitational terminal speed, Equation 10.3, is proportional to r^2. A lower prevailing wind speed will have the same effect.

Figure 10.18 (Kimoto et al., 1972) shows variation of ESDD on standard cap and pin discs, with distance from an industrial pollution source emitting soot and smoke. It is shown that pollution severity stabilizes at distance from the source below 5 km, which is an order of magnitude shorter than corresponding distances from the seacoast reported earlier. This may be attributed to the fact that for a point source, the pollutant content in air decays with approximately the square of the distance from the source.

10.3.3.7 Effect of Wind Speed

As mentioned previously, the effect of wind on insulator pollution buildup is quite complex acting both as the medium carrying airborne deposit and as a self-cleaning agent. Let us assume that the salt deposit density, ESDD mg/cm^2, for any insulator design, is a function of the salt density per unit volume in air, D_s, g/m^3; mean wind speed v_w, m/s; and exposure time t:

$$\text{ESDD} = F\left(D_s, v_w, t\right) \tag{10.10}$$

By dimensional analysis (Langhaar, 1951), intuition yields one dimensionless variable so that

$$Y\left[\frac{\text{ESDD}}{D_s v_w t}\right] = 0 \tag{10.11}$$

or

$$\text{ESDD} = K_s D_s \cdot v_w \cdot t \tag{10.12}$$

where K_s is a constant depending on insulator profile, which can only be determined by experiment.

From (10.12), if the volume density of salt in air is independent of v_w, then ESDD will be proportional to both mean wind speed and exposure time t. An investigation of marine pollution in Japan (Taniguchi et al., 1979), however, has shown that D_s is proportional to the square of mean wind speed so that in such situation:

$$\text{ESDD} = K_s v_w^3 \cdot t \tag{10.13}$$

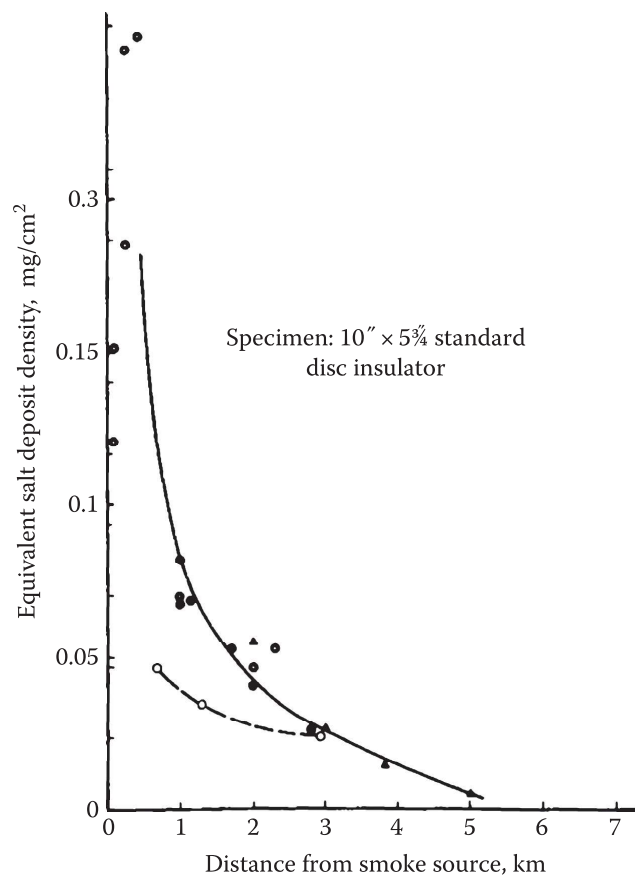The trend expressed by (10.13) is shown in Figure 10.19 (Taniguchi et al., 1979).

FIGURE 10.18 Example of relation of ESDD to the distance from smoke source under industrial pollution measured at various places. (From Kimoto, I. et al., *IEEE Trans. Power Appar. Syst.*, 91, 317, January 1972.)
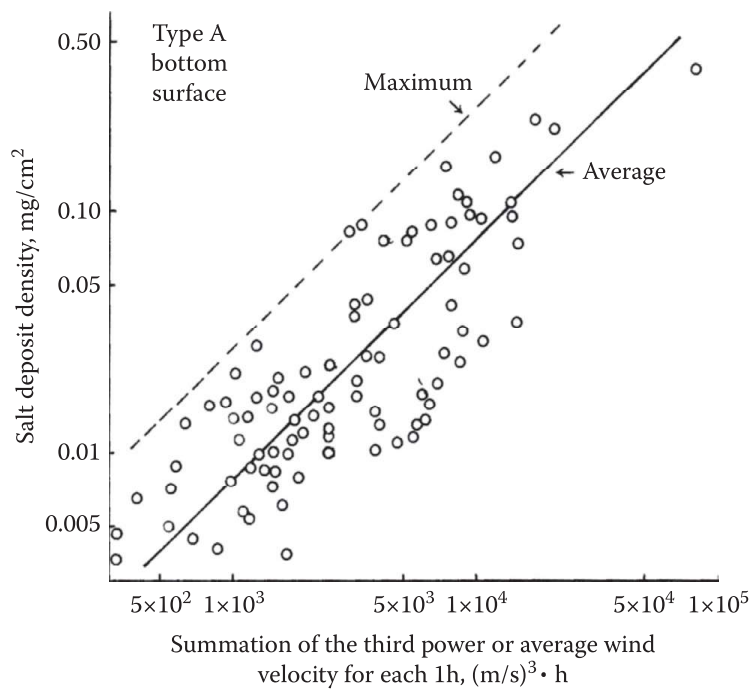

FIGURE 10.19 Variation of salt deposit density with average wind speed in marine environment. (From Taniguchi, Y. et al., *IEEE Trans. Power Appar. Syst.*, 98(1), 239, January/February 1979.)

Unfortunately, no similar field investigation of the dependence of ESDD on v_w was reported for other environmental conditions nor was such investigation undertaken in wind tunnel experiments (Hall and Mauldin, 1981). The effect of wind speed on wetting and insulator flashover will be treated in other sections.

10.3.3.8 Insulator Surface Wetting

10.3.3.8.1 Ceramic Insulator

As previously mentioned, wetting of the contamination layer is a prerequisite for flashover to occur. The most significant mechanisms for wetting of a predeposited layer include

- Adsorption of water from humid air due to the hygroscopic nature of salt contaminants
- Condensation by contact cooling leading to dew formation
- Precipitation in the form of drizzle

A systematic investigation *of wetting due* to the two first earlier mechanisms was reported in Rizk et al. (1975). Hygroscopic wetting was produced by exposing a contamination layer deposited on a glass plate to humidity in a special chamber. Constant humidity was maintained in the chamber by using different saturated aqueous solutions. A sample of the results is presented in Figure 10.20 showing variation of the specific layer conductivity of two contamination layers with exposure time in a constant relative humidity of 96%, at an ambient temperature of 20°C. The 40 and 72 μS values correspond to saturation values of these two layers when exposed for sufficient time to 100% relative humidity at 20°C. It is shown that the specific layer conductivity first increases rapidly, followed by a much slower rate to reach saturation. It is concluded that, when the contamination layer temperature is in equilibrium with the ambient atmosphere, hygroscopic absorption is a slow process with maximum surface conductivity reached in 1 h or more.

Figure 10.21 (Rizk et al., 1975) shows variation of the final surface layer conductivity, for the two layers mentioned earlier, with ambient relative humidity in the range of 67%–100%. It is shown that adsorption will lead to significant specific layer conductivity if the ambient humidity exceeds 85%.

Figure 10.22 (Rizk et al., 1975) shows a typical daily variation of ambient and insulator surface temperature of cap and pin and long-rod porcelain insulators in a desert environment. It is shown that in the early morning hours, insulator temperature can drop below the ambient temperature due to thermal inertia of the insulator. Although such temperature difference is around 2°C, this will be sufficient to cause dew formation on the insulator surface for ambient humidity below 90%, as shown in leakage current measurements of Figure 10.23 (Rizk et al., 1975). Here, a 2.2°C undercooling leads to very significant increase in the leakage current, starting with ambient relative humidity of 80%. Dew point was reached on the insulator surface at a relative humidity of 87.5% and saturation of the leakage current was attained at 92% of relative humidity. It is concluded that, in desert environment, undercooling of insulators in the early morning hours can lead to severe wetting of the pollution layer by dew formation, constituting a serious hazard for insulator flashover.
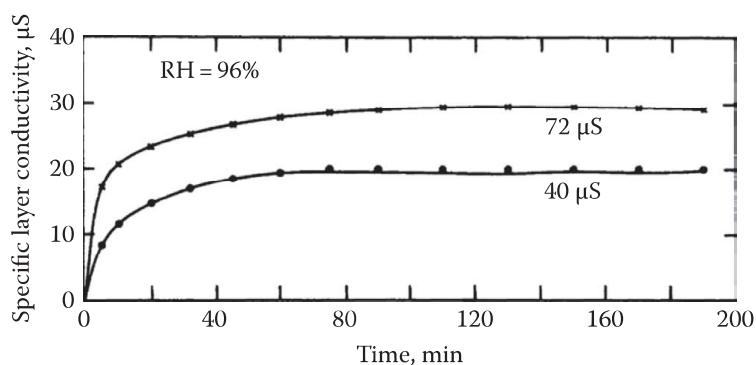

FIGURE 10.20   Response of natural desert contamination layers to ambient relative humidity at 20°C, relative humidity 96%. (From Rizk, F.A.M. et al., *IEEE Trans. Power Appar. Syst.*, 94(5), 1170, September/October 1975.)
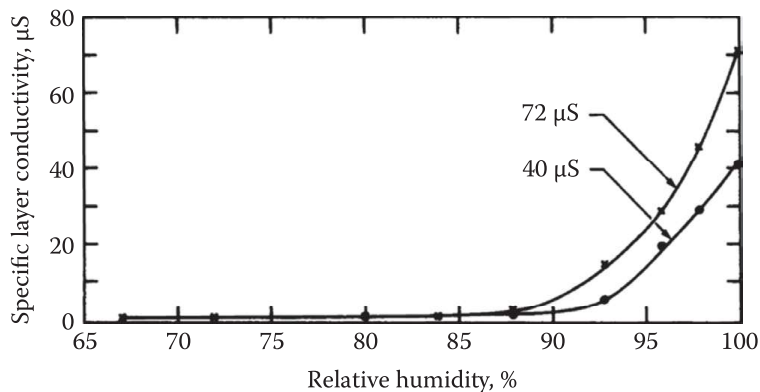
FIGURE 10.21 Variation of ultimate specific layer conductivity with ambient relative humidity at 20°C. (From Rizk, F.A.M. et al., *IEEE Trans. Power Appar. Syst.*, 94(5), 1170, September/October 1975.)
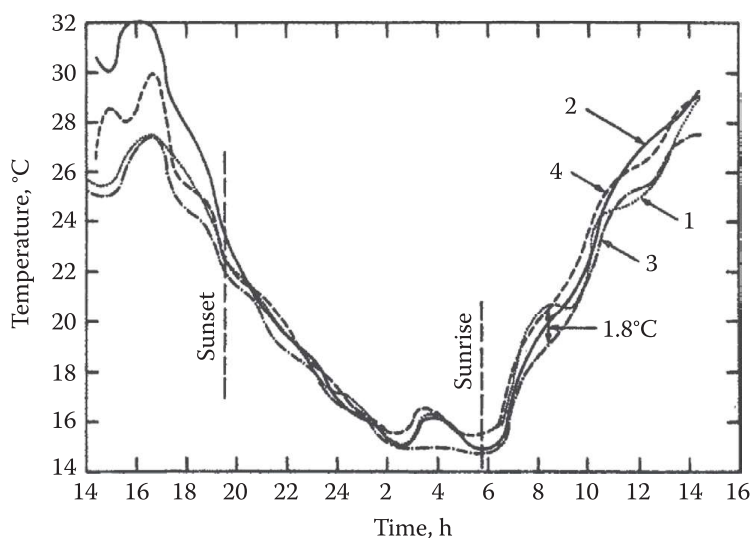

FIGURE 10.22 Typical daily variation of ambient and insulator temperature in the desert. 1—ambient temperature; 2—shed of disc insulator; 3—stem of 75/14 long rod; 4—shed of 75/14 long rod. (From Rizk, F.A.M. et al., *IEEE Trans. Power Appar. Syst.*, 94(5), 1170, September/October 1975.)
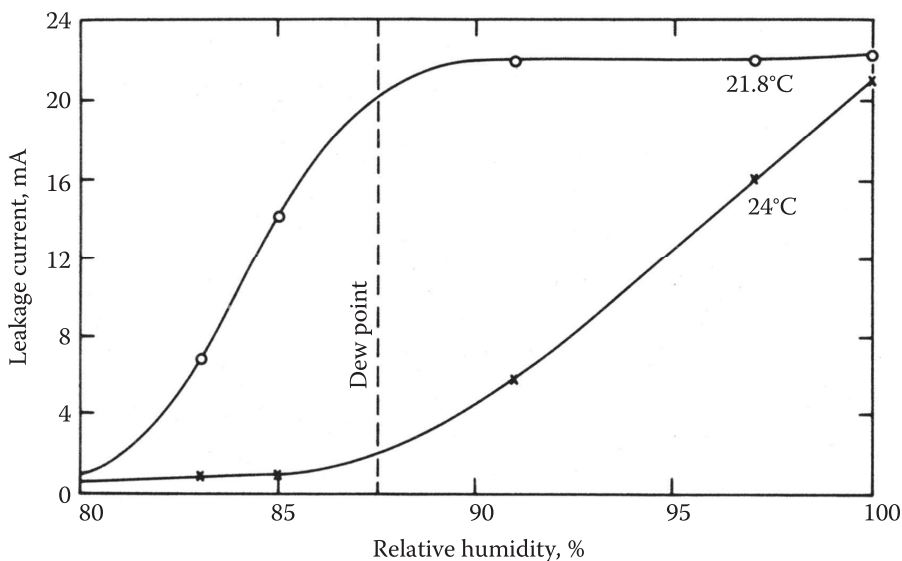

FIGURE 10.23 Variation of leakage current with relative humidity with and without under cooling. (From Rizk, F.A.M. et al. Laboratory and field experience with EHV transmission line experience in the desert. *IEEE Trans.*, Vol. PAS-94, No. 5, pp. 1770–1776, September/ October 1975.)
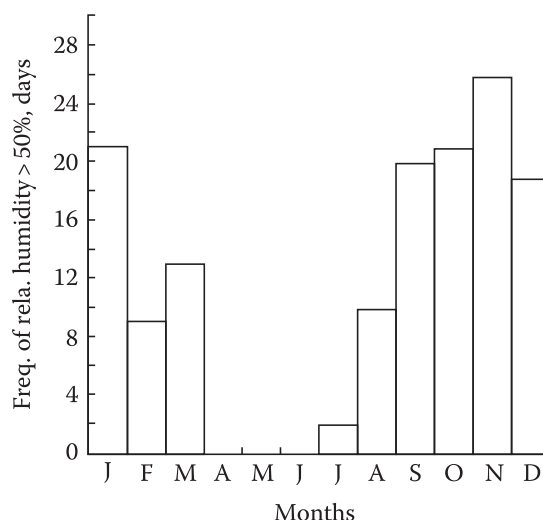
FIGURE 10.24 Days with relative humidity exceeding 90% at El-Minya, Egypt. (From El-Koshairy, M.A.B. and Rizk, F.A.M., Performance of EHV transmission line insulators under desert pollution conditions, CIGRE, Paper No. 33-05, 1970.)

Insulator wetting in a clean fog chamber used for high-voltage testing of polluted insulators was analyzed by Karady (1975). It was shown that for cold fog, the major wetting factor is the collision of water drops with the insulator surface. For steam fog, on the other hand, condensation is the major factor. In case of warm fog, both condensation and water drop collision play a role in the wetting process. It was also shown that the condensation becomes more effective the lower the ratio between the insulator surface area and insulator thermal capacity (Karady, 1975).

Drizzle also can constitute a hazardous wetting agent for contaminated insulators. Typical parameters of drizzle (Humphreys, 1964) include a precipitation rate of 0.25 mm/h, yielding 0.4 mg/cm²/min, a droplet radius of 100 μm, and water content in air of 90 mg/m³. It may be interesting to compare these drizzle parameters with corresponding parameters in a fog chamber described in Karady (1975).

The following are noted:

- The drop size in drizzle is an order of magnitude larger than that of condensation water drops in the fog chamber.
- The drizzle precipitation rate of 0.4 mg/cm²/min is smaller than the typical rate of 1 mg/cm²/min in the fog chamber (Karady, 1975).
- The water content of typically 40 g/m³ in the fog chamber (Naito and Nagasaka, 1975) is three orders of magnitude higher than the corresponding value of 90 mg/m³ in atmospheric air associated with drizzle.

It should be noted that the effect of dew formation on polluted insulators is by no means confined to desert conditions and has been earlier accounted for in Europe (Wittenzellner, 1962).

It can be understood from the earlier texts that the frequency of occurrence of days with 90% relative humidity can be used as a measure of wetting events on polluted insulators (El-Koshairy and Rizk, 1970). Figure 10.24 shows a histogram of days of relative humidity exceeding 90% at El-Minya, Egypt. It should be noted that pollution flashover is a slow process and, accordingly, it is not sufficient that high-humidity conditions occur but that such conditions last for 1–2 h to constitute a serious hazard (Rizk et al., 1975).

10.3.3.8.2 Nonceramic Insulators

It is obvious that the wetting agents of fog, dew, drizzle, etc., will be the same for polymeric insulators as for porcelain and glass. The justification of treating this in a separate section, however, is the different response of the polymeric surface to wetting. When a clean high-energy surface like porcelain or glass is exposed to sufficient wetting, it forms a continuous layer of water (Rizk, 1974; Rizk and Hyltén-Cavallius, 1974). A polymeric surface, on the other hand, forms isolated drops manifesting a property termed hydrophobicity (Vlastos and Sherif, 1990). One index for evaluating hydrophobicity is
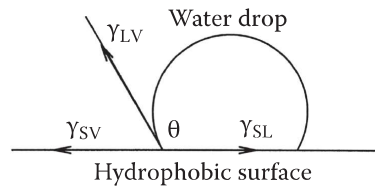
FIGURE 10.25 Schematic diagram of a water drop on a hydrophobic surface.

the contact angle θ at the triple point between a water drop, a solid substrate (polymer), and vapor (air) in Figure 10.25. The contact angle is determined by the balance of surface tension γ_{LV} (liquid/vapor), γ_{SL} (solid/liquid), and γ_{SV} (solid/vapor) as expressed by the Young–Dupré equation (Adamson, 1967):

$$\gamma_{LV} \cos\theta = \gamma_{SV} - \gamma_{SL} \tag{10.14}$$

which is valid for a perfectly smooth surface.

Ultimately, for full wetting as $\theta \to 180°$, (10.14) yields

$$\gamma_{LV} + \gamma_{SV} = \gamma_{SL} \tag{10.15}$$

The practical problem with (10.14) is that both γ_{SV} and γ_{SL} cannot be measured or calculated. The contact angle θ can be measured by

- Direct photography of small droplets (~10 μm) placed on a horizontal substrate (Vlastos and Sherif, 1990)
- Direct photographic determination as the difference between advancing and receding contact angles on an inclined plane substrate (Pigini and Tomba, 1993)
- Direct photography of the meniscus rise h (Morcos and Rizk, 1977) at a substrate plate or cylindrical solid (polymer) partially immersed in a liquid (water) expressed by

$$\sin\theta = 1 - \frac{\rho g}{\gamma_{LV}} h^2 \tag{10.16}$$

where
ρ is the liquid density
g is the acceleration of gravity

- Practical evaluation of hydrophobicity by visual comparison of the pattern of water drop formation on an insulating surface to a given set of seven classes HC1 to HC7 (STRI, 1992)

It is presently understood that hydrophobicity is related to the presence of a layer of low molecular weight (LMW) silicon oil on the insulator surface (Chang and Gorur, 1994). Hydrophobicity is lost by corona and dry-band arcing but can be recovered as the LMW oil diffuses back to the surface from the polymer bulk (Chang and Gorur, 1994). It is clear that in the field at least temporary loss of hydrophobicity could also take place due to heavy rain, sandstorms, etc. It is also clear that if hydrophobicity is lost, wetting of polymeric insulators becomes similar to wetting of ceramic insulators. In this respect, it may be mentioned that in artificial pollution testing, several methods are used to *condition* the polymeric insulator in order to facilitate application of the wet contaminant. In effect, conditioning induces a temporary loss of hydrophobicity.

10.3.3.9 Pollution Flashover Mechanism

10.3.3.9.1 General Description

Excellent descriptions of the different phases involved in the pollution flashover mechanism, with special reference to ceramic insulators, were presented by Nasser (1962, 1972). This starts with a conducting layer already formed on the insulator surface and accounts for the complex interaction between

TABLE 10.6

Phases of Contamination Flashover Based on Nasser's Results

Phase	Layer	Discharge Form	Leakage Current
Heating of surface layer	Conductivity increases	None	Increases
Drying of surface layer	Conductivity decreases locally	None	Decreases
Dry zone formation	Lateral drying locally	None	Stops
Onset of dry zone arcing	Conductivity decreases	Bright laterally moving arcs	Intermittent surges
Glow and streamer discharges	Conductivity increases	Hardly visible discharges, radio noise	Very small and pulsating
Slow arc growth	Dry zones enlarged	Merging of arcs and slow arc growth	Increases slowly, intermittent
Fast arc growth	No further drying	Arc spans half of the insulator	Continuous, rapidly increasing
Flashover	Partly dried out	Arc	Short-circuit current

Source: Nasser, E., *ETZ-A*, 93(6), 321, 1972.

such layer and the applied voltage. Under critical conditions, such interaction will lead to full flashover. Table 10.6 is based on Nasser (1972) and summarizes the different phases, state of the contamination layer, form of electrical discharges, and corresponding leakage current.

In the more practical situation, layer formation and wetting take place under voltage, but most of the phases described in Table 10.6 remain valid, with differences only in the initial phases before maximum layer conductivity is reached.

In another publication (Nasser, 1968), Nasser described a systematic investigation involving synchronized photographic and oscillographic recording of the glow, streamer, and arc discharges on polluted surfaces.

There are some fundamental differences in the phases of pollution flashover of silicone rubber insulators. Firstly, it should be noted that the pollutant will be embedded in the LMW silicon oil on the insulator surface. The second point is that the initial wetting mostly comprises isolated water drops on the surface of the energized insulator. Karady et al. (1995) suggested a sequence of events that may lead to flashover of silicone rubber insulators:

- The first phase involves migration of the pollutant to the water droplets or migration of water into the dry pollutant.
- In both previous cases, a continuous layer is formed and, through the flow of a relatively small leakage current, ohmic heating occurs.
- As wetting continues, the surface density of the droplets increases and the interdroplet distance is reduced.
- Also under the effect of the electric field, droplets may elongate forming conducting filaments.
- Filaments intensify the electric field at their tips and initiate spot discharges.
- Discharges lead to loss of the LMW polymer layer and results in loss of hydrophobicity.
- Wet regions start to form as a result of local hydrophobicity loss.
- Formation of the wet regions and elongation of the filaments create a path for arc propagation similar to the ceramic insulators.

10.3.3.9.2 Pollution Layer Resistance

Consider an insulator with a wet pollution layer having a volume resistivity ρ, in $\Omega \cdot m$, and layer height h; the surface conductivity χ_s will then be given by

$$c_s = \frac{h}{r} \tag{10.17}$$

The layer resistance per unit leakage path length $r(s)$ will be expressed as

$$r(s) = \frac{1}{\pi D(s) \chi_s} \tag{10.18}$$

where $D(s)$ is the insulator diameter at a leakage distance S from one end. The total pollution resistance R_p can be expressed as

$$R_p = \int_0^L \frac{ds}{\pi D(s) \chi_s} \tag{10.19}$$

where L is the total leakage path.

If χ_s is assumed constant along the leakage path,

$$R_p = \frac{1}{\chi_s} \int_0^L \frac{ds}{\pi D(s)} \tag{10.20}$$

The integral in (10.20) is a geometric parameter termed the insulator form factor f with

$$f = \int_0^L \frac{ds}{\pi D(s)} \tag{10.21}$$

which can also be expressed as

$$f = \frac{L}{\pi D_{av}} \tag{10.22}$$

where D_{av} is the insulator average diameter.

It is clear that the form factor is proportional to the leakage path and inversely proportional to the average diameter. From (10.20) and (10.21), we get

$$R_p = \frac{f}{\chi_s} \tag{10.23}$$

relating the total pollution resistance to the form factor and surface conductivity.

When the pollution layer is characterized by the ESDD, mg/cm², it would be helpful to correlate ESDD with the specific layer conductivity χ_s. Such equivalence can only be established on the basis of equality of the insulator withstand voltage under a defined test technique.

It should be noted that the electrical conductivity of an electrolytic solution increases substantially with temperature so that at 100°C, it is roughly three times higher than at 20°C.

10.3.3.9.3 Slow Arc Growth

As indicated in Table 10.6, heating of the surface layer due to leakage current flow results in increased conductivity. Energy dissipation is obviously more intense in regions of smallest diameter. As boiling temperature is reached in those reasons, intense evaporation occurs resulting in substantial reduction in the layer thickness, leading to dry-band formation. Modeling of dry-band formation and growth is reported in Loberg (1971) and Raghuveer and Kuffel (1974). Dry-band arcing is a prerequisite for pollution flashover under service voltage. However, under field conditions, it normally takes place at leakage current levels substantially lower than the critical levels required for flashover. In Table 10.6, thermal growth of dry-band arcs is referred to as slow, resulting in merging of arcs and characterized by slow increase of intermittent leakage current. Only when this phase is followed by fast arc growth can a significant risk of flashover be expected.

10.3.3.9.4 Fast Arc Growth

The mechanism of fast arc growth over the surface of a polluted insulator has been the subject of several investigations. It may be helpful to start reviewing the different types of forces that could be exerted on an electric arc. We will then reflect on which among those forces could be a plausible cause for arc propagation:

- Thermal buoyancy forces are particularly relevant to horizontal arcs, driving the arc upward, making the actual arc length significantly longer than the shortest distance between terminal electrodes. It would be difficult, however, to see how buoyancy forces could be responsible for arc propagation on a contaminated insulator surface.

- Magnetic (Lorentz) forces can in principle displace electric arcs. However, the low levels of leakage current, in the range of a fraction of an ampere to a few amps, make such forces unlikely to play a significant role in arc propagation over a polluted insulator surface.

- Electrostatic forces have been proposed as responsible for the fast arc growth phase (Nasser, 1972). This will be discussed further in the following. It should be mentioned, however, that the arc column is quasi-neutral, with practically equal density of electrons and positive ions. Electrostatic forces, therefore, can only act on the arc cathode or anode regions where a net charge is available (Engel, 1955). A net electrostatic force on such charge would drag the arc cathode or anode region towards the counter electrode over the polluted insulator surface.

- Ionization in air in the vicinity of the arc root, although not constituting a mechanical force acting on the arc, has been suggested as a viable mechanism for arc extension (Obenaus et al., 1965; Wilkins and Baghdadi, 1971).

Hampton (1964) conducted flashover experiments on a uniform water column with practically constant resistance per unit length. The criterion for arc motion was formulated as

$$E_a < E_p \tag{10.24}$$

where
E_a is the (mean) arc voltage gradient
E_p is the (mean) voltage gradient in the pollution layer

Hesketh (1967) suggested that an arc burning in series with a wet pollution layer will adjust itself, without specifying the mechanism, to draw maximum current from the supply. The criterion for arc propagation then reads

$$\frac{\mathrm{d}i}{\mathrm{d}x} > 0 \tag{10.25}$$

where
i is the arc current
x is the arc length

Consider a source with voltage U and internal resistance R_s, applied to a polluted insulator. The circuit equation will be

$$U = \left(R_s + R_p\right)i + xE_a \tag{10.26}$$

where
x is the arc length
E_a is the arc voltage gradient
R_p is the pollution resistance
i is the leakage current

Differentiating (10.26) with respect to x, Hesketh used (10.25) to obtain

$$\frac{E_a + i(\mathrm{d}R_p/\mathrm{d}x)}{x(\mathrm{d}E_a/\mathrm{d}i) + R_p + R_s} < 0 \tag{10.27}$$

If the denominator in (10.27) is positive, the numerator results in

$$E_a < -i\frac{dR_p}{dx} \tag{10.28}$$

Since $E_p(x) = -i(dR_p/dx)$, Hesketh's criterion becomes

$$E_a < E_p(x) \tag{10.29}$$

The difference from (10.24) is that (10.29) applies to the case of a nonuniform pollution resistance and expresses a local condition for arc propagation.

10.3.3.9.5 Pollution Resistance during Arc Growth

Consider a polluted insulator energized with a voltage U. An arc of length x is burning in series with a layer resistance R_{px}. The simple circuit equation will show that the value and distribution of R_{px} will be determining both the arc current i and the pollution voltage gradient E_p, which, according to the earlier criterion, will decide whether the criterion for arc propagation will be satisfied. Furthermore, as will be shown in the following, R_{px} will also be decisive for determining the critical voltage U_c needed to maintain the arc of any length on the insulator surface. Knowing R_{px} is therefore essential for modeling the flashover process. Exact knowledge of the value and distribution of the dynamic layer resistance R_{px} during the arc propagation is difficult due to the following reasons:

- Even with a uniform pollution surface conductivity or salt deposit density, the insulator geometry makes the distribution of R_{px} quite complex (IEC Standard 60507, 1991).
- Under field conditions, the surface conductivity is usually far from uniform (Rizk et al., 1975) with at least vastly different values on the upper and bottom insulator surfaces.
- The arc itself contributes to the complexity of the situation: firstly, through constriction at the arc foot points, and, secondly, through the resulting thermal effects influencing the layer conductivity.
- For insulators with large diameter, particularly supporting columns, parallel arcing may persist resulting in a complex pattern.

It is therefore understandable that, for modeling of the flashover process, several models were put forward to represent the pollution surface resistance. These models differ widely in their complexity. Even with much simplification, such models contribute to our basic understanding of the underlying phenomena and interpretation of test results.

The simplest model was suggested by Neumärker (1959), with a constant pollution resistance r_p per unit leakage length yielding R_{px} as

$$R_{px} = r_p(L - x) \tag{10.30}$$

where
  L is the leakage path length
  x the arc length

From a practical point of view, r_p can be taken as the average pollution resistance per unit length:

$$\overline{r_p} = \frac{R_p}{L} = \frac{f}{c_s L} \tag{10.31}$$

where
  R_p is the total pollution resistance for the length L
  χ_s is the layer surface conductivity, assumed constant
  f is the insulator form factor

Böhme and Obenaus (1966) considered two series resistive layers characterizing the stem and shed zones of a long-rod insulator with leakage lengths l_1 and l_2 and corresponding to mean surface resistances per unit leakage length, $\overline{r_{p1}}$ and $\overline{r_{p2}}$, respectively.

Here the total leakage path $L = l_1 + l_2$. The total pollution layer resistance R_p is given by

$$R_p = \overline{r_{p1}}\,l_1 + \overline{r_{p2}}\,l_2 \tag{10.32}$$

If arcs with total length x are burning on the stem region, the series layer resistance R_{px} will be expressed as

$$R_{px} = \overline{r_{p1}}\,(l_1 - x) + \overline{r_{p2}}\,l_2 \tag{10.33}$$

For a circular insulating disc model, using the symbols of this chapter, Woodson and McElroy reported that pollution resistance R_{px} in series with an arc of length x may be expressed as

$$R_{px} = \frac{\text{const}}{c_s}\,(L - x)^m \tag{10.34}$$

with the exponent $m = 1.4$.

A possible reformulation of (10.34) suggested is

$$R_{px} = R_p\left(1 - \frac{x}{L}\right)^m \tag{10.35}$$

where R_p is the total pollution resistance as $x \to 0$.

Similarly, Claverie (1971) made measurements on a long-rod insulator and presented a relationship between R/ρ and the length x, as shown in Figure 10.26. Here, R is what has been designated R_{px} earlier and ρ is the volume resistivity of the liquid polluted of height h. As indicated in (10.17), $\chi_s = h/\rho$. Here again, the variation of R_{px} with x may be approximated as

$$R_{px} = R_p\left(1 - \frac{x}{L}\right)^m \tag{10.36}$$

where
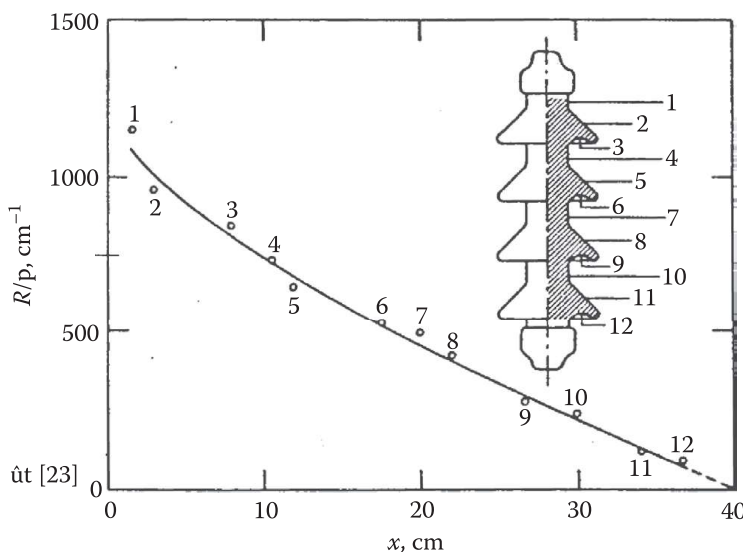R_p is the total pollution resistance
m is a constant

FIGURE 10.26 Distribution of pollution surface resistance of a long-rod insulator. (From Claverie, *IEEE Trans. Power Appar. Syst.*, 90(4), 1902, July/August 1971.)

It should be noted that in Woodson and McElroy (1970) and Claverie (1971), the resistance distribution and *m* value were necessarily determined using a metallic electrode, not an arc, so that the results may not be fully representative. In case of a cap and pin insulator unit, Claverie (1971) found that, due to under ribs, the variation of R_{px} with *x* is quite complex. It should be noted, however, that for long insulator strings during the phase of fast arc growth, the arc often bridges several insulator units, and the series pollution resistance R_{px} also refers to several discs. Under these circumstances, the variation of R_{px} with *x* will not be disturbed by the under ribs to the same extent as measurements on a single unit tend to indicate.

The effect of constriction of leakage current at the arc foot point was explicitly analyzed by Näcke (1969) and Wilkins (1969). Näcke (1969) considered a rectangular pollution strip of length x_p and width *b* with arc foot points represented by two semicircles of radius r_b.

For a narrow strip, the pollution layer resistance R_{px} can be expressed as

$$R_{px} = \frac{1}{\rho c_s} + \bar{r}_p x_p + \frac{2}{\rho c_s} \ln\left(\frac{b}{2\rho r_d}\right) \tag{10.37}$$

According to Näcke's analysis (Näcke, 1969), the first term in (10.37) refers to the internal resistance at the semicircular arc foot points, while the two other terms are referred to as the external resistance. For a wide strip, Näcke's results (Näcke, 1969) could be expressed as

$$R_{px} = \frac{1}{\rho c_s} + \frac{2}{\rho c_s}\left(0.3 + \ln\frac{x_p}{r_d}\right) \tag{10.37a}$$

From (10.37), it is clear that the wide strip pollution resistance is much less dependent on the strip length x_p than for a narrow strip (10.36).

Wilkins (1969) considered circular arc foot points and obtained results that are very similar to Näcke's. For a narrow strip, Wilkins obtained the following:

$$R_{px} = \bar{r}_p (L - x) + \frac{1}{\rho c_s} \ln\left(\frac{b}{2\rho r_d}\right) \tag{10.38}$$

The major difference with (10.37) due to Näcke (1969) is the absence of the internal resistance term at the arc foot points.

Substituting for $c_s = 1/(b\bar{r}_p)$, (10.38) becomes

$$R_{px} = \bar{r}_p (L - x) + \frac{b\bar{r}_p}{\rho} \ln\left(\frac{b}{2\rho r_d}\right) \tag{10.39}$$

To estimate the relative values of the two resistance terms on the right-hand side of (10.39), we will consider a numerical example. Consider a simple cylindrical insulator with length 100 cm and diameter 5 cm (*b* = 15.7 cm), with a uniform pollution layer of $\chi_s = 40$ μS. The arc diameter is assumed as 4 mm ($r_d = 2$ mm) and the arc length 50 cm.

$\bar{r}_p$ is obtained at 1592 Ω/cm. Substituting in (10.39),

$$\bar{r}_p (L - x) = 79.6 \text{ k}\Omega$$

and

$$\frac{b\bar{r}_p}{\rho} \ln\left(\frac{b}{2\rho r_d}\right) = 20.1 \text{ k}\Omega$$

The example shows that the increase in the pollution layer resistance due to constriction at the arc roots can be quite significant. An anode and cathode voltage drop of about 800 kV per arc could be added (Wilkins, 1969). This effect could be substantial if it is assumed that many arcs are simultaneously burning in series.

It should be noted that, during the dry-band phase, many arcs will be burning in series. Gradually, however, as the critical phase of fast arc propagation is reached, the number of series burning arcs drops substantially. Another point is that the region of high current density in the vicinity of the arc foot

point will necessarily have a higher temperature and, accordingly, increased electrical conductivity that will tend to suppress the earlier effect.

10.3.3.9.6 *Modeling of Flashover Characteristics*

10.3.3.9.6.1 DC Model   There are two conditions necessary for pollution flashover to occur: a mechanism for arc growth and sufficient applied voltage to maintain the arc in series with the pollution layer resistance. The first condition was expressed by (10.24). Consider the simple dc circuit of an arc of length x and current i burning in series with a pollution surface resistance R_{px} under an applied voltage U as in (10.26):

$$U\left(x,i\right) = xE_a + iR_{px} \tag{10.40}$$

Let

$$E_a = \frac{N_0}{i^n}$$

and

$$R_{px} = R_p \left\{ F \left[\frac{x}{L} \right] \right\} \tag{10.41}$$

with $F(0) = 1$ and $F(1) = 0$.

Substituting in (10.40),

$$U\left(x,i\right) = \frac{xN_0}{i^n} + i\left\{ R_p F \left[\frac{x}{L} \right] \right\} \tag{10.40a}$$

To maximize U, the following conditions must be satisfied:

$$\frac{dU}{dx} = 0 = \frac{N_0}{i^n} + iR_p \left\{ \frac{1}{L} F' \left[\frac{x}{L} \right] \right\} \tag{10.42}$$

$$\frac{dU}{di} = 0 = -n\frac{xN_0}{i^{n+1}} + R_p \left\{ F \left[\frac{x}{L} \right] \right\} \tag{10.43}$$

Note that from (10.41)

$$\frac{dR_{px}}{dx} = -r_{px} = \frac{R_p}{L} \left\{ F' \left[\frac{x}{L} \right] \right\} \tag{10.44}$$

where r_{px} is the local pollution resistance per unit length about to be bridged by the arc of length x. It follows that (10.42) for critical conditions can be expressed as

$$\frac{N_0}{i_c^n} - r_{px}i_c = 0$$

that is,

$$\frac{N_0}{i_c^n} = r_{px}i_c \tag{10.45}$$

or

$$E_a = E_p$$

which agrees with the criterion for arc motion (10.24).

Equations 10.42 and 10.43 should be solved to obtain the critical arc length x_c and critical leakage current i_c from which the critical flashover voltage U_c is determined.

Substituting from Equation 10.42 into Equation 10.43,

$$x_c = -\frac{L\,F\left(x_c/L\right)}{n\,F'\left(x_c/L\right)} \tag{10.46}$$

For the simplest case of a uniform pollution resistance r_p per unit leakage length,

$$F\left(\frac{x}{L}\right) = 1 - \frac{x}{L}$$

$$F'\left(\frac{x}{L}\right) = -1 \tag{10.47}$$

Substituting in (10.46),

$$x_c = \frac{L}{n}\left(1 - \frac{x_c}{L}\right)$$

or

$$x_c = \frac{L}{n+1} \tag{10.48}$$

With $n = 0.76$ (Wilkins, 1969),

$$x_c = 0.57\,L \tag{10.49}$$

which means that the arc has to span more than half of the leakage path for a flashover to occur.

Substituting for $F'(x/L) = -1$ in Equation 10.42, we get

$$\frac{N_o}{i_c^n} = i_c r_p \tag{10.50}$$

which is exactly the condition for arc motion (10.24), yielding

$$i_c = \left(\frac{N_o}{r_p}\right)^{1/(n+1)} \tag{10.51}$$

It is interesting to note that the critical current is independent of the leakage path.

Substituting for R_{px}, x_c, and i_c into (10.40), an expression for the critical flashover voltage U_c is obtained as

$$U_c = N_o^{1/(n+1)}\, r_p^{n/(n+1)}\, L \tag{10.52}$$

as previously obtained by Neumärker (1959).

Consider now the more general distribution of pollution layer resistance expressed by (10.35)

$$F\left(\frac{x}{L}\right) = \left(1 - \frac{x}{L}\right)^m$$

$$F'\left(\frac{x}{L}\right) = -m\left(1 - \frac{x}{L}\right)^{m-1} \tag{10.53}$$

which, when substituted in (10.46), gives

$$x_c = \frac{L - x_c}{nm} \quad \text{or} \quad x_c = \frac{L}{1 + nm} \tag{10.54}$$

As a numerical example, take as before $n = 0.76$ and $m = 1.4$:

$$x_c = 0.48\, L$$

which is slightly less than the critical arc length of the uniform pollution resistance case (10.49) but still close to half of the leakage path.

Substituting for x_c in (10.45), an expression for the critical current i_c is obtained as

$$i_c = K_i \left(\frac{\hat{E}N_o}{r_p}\right)^{1/(n+1)} \tag{10.55}$$

where

$$K_i = \frac{1}{m^{m/(n+1)}} \left(\frac{1 + n\langle\rangle m}{n}\right)^{(m-1)/(n+1)} \tag{10.56}$$

so that i_c differs from the uniform pollution case by the constant K_i. It is obvious that the uniform pollution case follows by letting $m = 1$, which yields $K = 1$.

As a numerical example, with $N = 0.76$ and $m = 1.4$, the constant K_i is obtained at 0.96 so that the critical leakage current has been reduced insignificantly by the generalized distribution of pollution resistance (10.35).

Substituting for x_c and i_c in (10.40), the critical voltage U_c is obtained at

$$U_c = K_u N_o^{1/(n+1)} \left(\overline{r_p}\right)^{-n/(n+1)} \langle\rangle L \tag{10.57}$$

where K_u is a constant expressed as

$$K_u = \frac{1}{\left(1 + n\langle\rangle m\right)} \left[\frac{1}{K_i^n} + n\langle\rangle m\right] \tag{10.58}$$

With $n = 0.76$ and $m = 1.4$ as earlier, $K_i = 0.96$ and $K_u = 1.016$. This indicates that, with the earlier constants, the critical flashover voltage was slightly changed by using the nonlinear pollution resistance distribution (10.35) rather than the simple uniform distribution. It is clear from (10.58) that as $m \to 1$, $K_u \to 1$ as to be expected.

10.3.3.9.6.2 AC Models It has long been known that the withstand level of a polluted insulator under alternating voltage (ac) is substantially higher than under direct voltage (dc) (Forrest, 1969; Lambeth, 1971). The basic reason is that while the condition of arc propagation may be satisfied, extinctions at current zeros require a higher voltage to maintain an ac arc. The analysis of the mechanism of recovery and reignition of ac arcs on a polluted insulator has first been undertaken by Rizk (1971). A review of this analysis is further included in Rizk (1981) and Rizk and Nguyen (1984). The significance of the reignition characteristics of ac arcs on polluted insulators has also been stressed by Claverie (1971), based on tests of cap and pin and long-rod insulators.

In Rizk (1971), dielectric recovery of a free-burning arc in air was analyzed on the basis of an approximate solution of the energy balance equation of the residual arc plasma subsequent to a current zero. For an arc peak current i, length x, and time t after current zero, the instantaneous dielectric recovery voltage U_d (x, i, t), from the Rizk model with updated thermal conductivity values for air, can be expressed as (Rizk and Rezazada, 1997)

$$U_d\left(x,i,t\right) = xE_d\left(t\right) = xE_{d0}\left[1 + \frac{64.69}{1 + \left(211.3t/i^{1.326}\right)}\right]^{-0.562} \tag{10.59}$$

where E_{d0} is the power frequency dielectric strength of the arc gap, without current, at room temperature, assumed to be in the range of 5–6 kV_{peak}/cm.
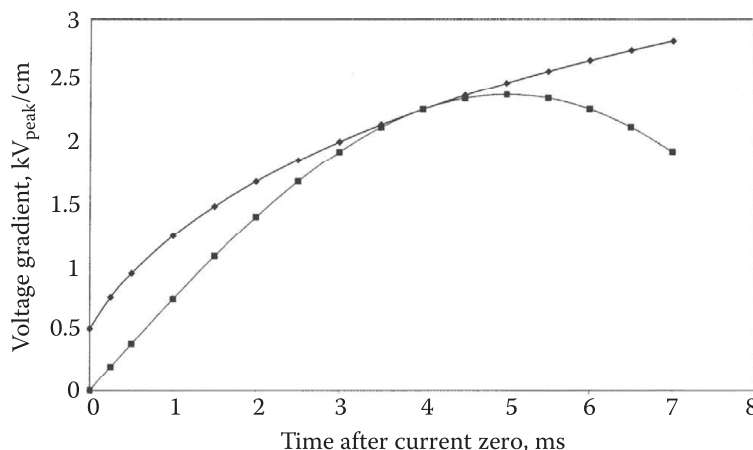
FIGURE 10.27   Determination of arc reignition characteristics: upper curve dielectric strength $E_d(t)$; lower curve: 50 Hz applied recovery voltage gradient $E_{ds}(t)$. I = 0.1 A; E_{sc} = 2395 V_{peak}/cm.

Variation of the instantaneous reignition voltage gradient $E_d(t)$ can, by definition, be obtained from (10.59) as $U_d(t)/x$. This equation has to be solved with the sinusoidal applied voltage to determine the critical reignition supply peak voltage (Figure 10.27).

Figure 10.28 shows variation of the reignition peak supply voltage gradient E_{ds} with arc current in the range 0.1–2.0 A, assuming E_{do} = 5.25 kV_{peak}/cm. It is shown that, for a leakage current of 0.1 A, E_{ds} = 2395 V_{peak}/cm or 1694 V_{rms}/cm, while the corresponding values for a 2.0 A arc are E_{ds} = 604 V_{peak}/cm or 427 V_{rms}/cm.

Within a certain range of leakage current, the peak reignition supply voltage gradient E_{ds} can be expressed in the form

$$E_{ds} = \frac{A}{i^a} \tag{10.60}$$

where A and α are constants. It should be noted that our interest is in the minimum values of the reignition supply voltage gradient needed to reestablish the arc, leading to continued arc propagation.

Regression analysis of the results of Figure 10.28 shows that for $0.1 \le i \le 1$ A, with R-square of 0.996, α = 0.52 and A = 698 V_{peak}/cm. Extending the regression range to $0.1 \le i \le 2$ A, it was found that R-square was reduced to 0.984, with also a lower α = 0.47 while A = 751 V_{peak}/cm.

Experimental results in Claverie (1971) yielded an exponent α of the reignition characteristics amounting to 0.5, in good agreement with the Rizk model results. In Claverie (1971), the constant A was determined as 940 V_{peak}/cm, but in Claverie and Porcheron (1973), this constant was reduced
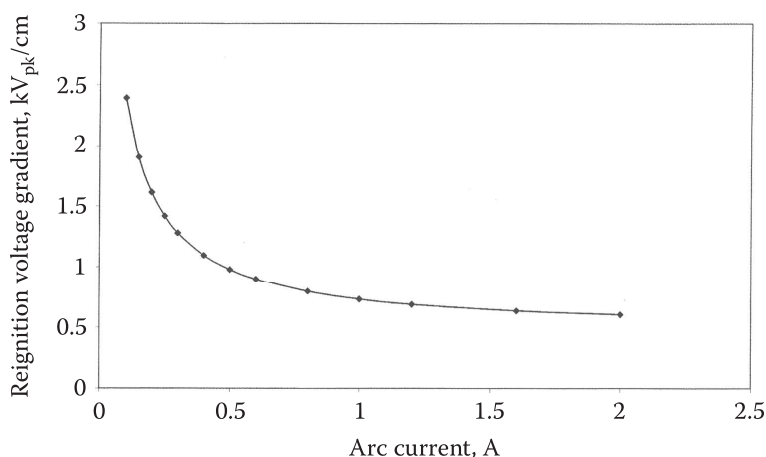

FIGURE 10.28   Variation of power frequency reignition voltage gradient E_{ds} of free-burning arc in air with arc current according to the Rizk model.

to 800 V_{peak}/cm. These values were based on fitting of flashover characteristics of different insulator designs. It was previously suggested (Rizk, 1981) that fitting should have been made in Claverie and Porcheron (1973) with minimum instead of mean flashover voltages, which would have resulted in A close to 700 V_{peak}/cm. The earlier values are in reasonably good agreement with the model.

For the determination of the critical ac supply voltage for flashover of polluted insulators, two equations have to be considered. The first is the circuit equation at the peak arc current i and length x in series with the pollution surface resistance R_{px} under the peak supply voltage $U_s(i, x)$:

$$U_s\left(i,x\right)=\frac{xN_o}{i^n}+iR_{px} \tag{10.61}$$

The second equation to be satisfied is the arc reignition condition:

$$U_s\left(i,x\right)=\frac{xA}{i^a} \tag{10.62}$$

As mentioned previously, R_{px} will be expressed as

$$R_{px}=R_p\left(1-\frac{x}{L}\right)^m=\overline{r_p}\left(L\left(1-\frac{x}{L}\right)^m\right) \tag{10.63}$$

where
$\overline{r_p}$ is the average pollution resistance per unit leakage length
L is the leakage path

Equations 10.61 and 10.62 can be solved numerically, but with some minor simplification, an analytic solution could be obtained. Since the arc voltage drop is much lower than its dielectric reignition voltage, it can be taken as an approximation that $n = \alpha$. Substituting for U_s from (10.62) into (10.61),

$$\frac{\left(A-N_o\right)x}{i^a}=i\overline{r_p}L\left(1-\frac{x}{L}\right)^m \tag{10.64}$$

yielding an expression for the variation of i as function of x:

$$i^{a+1}=\frac{\left(A-N_o\right)x}{\overline{r_p}L\left(1-\frac{x}{L}\right)^m} \tag{10.65}$$

Substituting from (10.65) into (10.62), an expression for the required supply voltage to maintain an arc of length x over this insulator is obtained:

$$U_s\left(x\right)=\frac{A}{\left(A-N_o\right)^{a/(1+a)}}x^{1/(1+a)}\left(\overline{r_p}^{a/(1+a)}\right)\left(L^{a/(1+a)}\left(1-\frac{x}{L}\right)^{(ma)/(1+a)}\right) \tag{10.66}$$

The critical flashover voltage U_{sc} can be obtained by maximizing U_s with respect to x, which will first result in an expression for the critical arc length x_c:

$$x_c=\frac{L}{\left(1+ma\right)} \tag{10.67}$$

which, for the linear model with $m = 1$, yields the familiar expression

$$x_c=\frac{L}{\left(1+a\right)} \tag{10.67a}$$

Substituting for x_c in (10.35) results in an expression for the critical leakage current i_c:

$$i_c = K_i \left(\frac{\bar{E}A - N_o}{\bar{r}_p} \right)^{1/(1+a)}$$ (10.68)

where for ac

$$K_i = \frac{(1 + ma)^{(m-1)/(1+a)}}{(ma)^{m/(1+a)}}$$ (10.69)

which, for the linear model with $m = 1$, becomes

$$K_i = \frac{1}{a^{1/(1+a)}}$$ (10.69a)

If $m = 1.4$ and $\alpha = 0.5$, (10.67) yields $x_c/L = 0.588$ while for the linear model of pollution resistance with $m = 1$, $x/L = 0.667$. It can therefore be concluded by comparison with dc model that the relative critical arc length is in general somewhat longer for ac than for dc and, here again, the nonlinear distribution of pollution resistance reduces the relative critical arc length.

Substituting for i_c and x_c in (10.62), an expression for the ac critical flashover (withstand) voltage is obtained:

$$U_{sc} = K_u A^{1/(1+a)} \left(\bar{r}_p \right)^{-a/(1+a)} L$$ (10.70)

where for ac

$$K_u = \frac{1}{\frac{\hat{E}}{\bar{E}} \left(1 - \frac{N_o}{A} \right)^{a/(1+a)} \left(K_i^a (1 + ma) \right)}$$ (10.71)

which, for the linear model with $m = 1$, becomes

$$K_u = \frac{a^{a/(1+a)}}{(1 + a) \left(\frac{\hat{E}}{\bar{E}} \right) \left(1 - \frac{N_o}{A} \right)^{a/(1+a)}}$$ (10.71a)

Some examples for the application of the model are given in the following.

Figure 10.29 shows the dependence of the critical leakage current on the average pollution surface resistance, with the linear model, $m = 1$, according to (10.68). It is shown that the critical leakage current
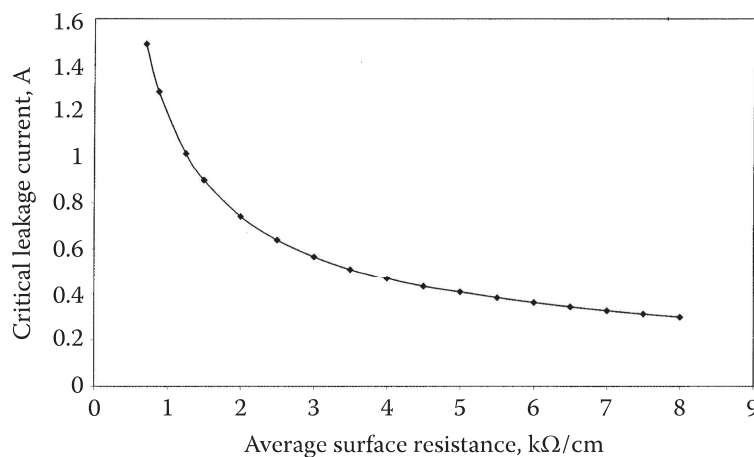

FIGURE 10.29 Variation of critical ac leakage current with average pollution surface resistance per unit leakage length.

is sensitive to pollution severity. For $\overline{r_p} = 700$ W /cm, $i_c = 1.49$ A, while for $\overline{r_p} = 7000$ W /cm, $i_c = 0.30$ A. This is consistent with the long established practice of using leakage current level to characterize pollution severity, as mentioned previously.

Figure 10.30 shows variation, again for the linear model, of the critical flashover voltage gradient E_{sc} with r_p in the range 700–8000 Ω/cm, according to (10.70). It is shown that E_{sc} varied from 382 V_{peak}/cm at $\overline{r_p} = 700$ W /cm to 861 V_{peak}/cm for $\overline{r_p} = 8000$ W /cm.

Finally, the linear model was used to predict pollution performance of a porcelain long-rod insulator-type VKL 75/14 with leakage path $L = 180$ cm and a form factor $f = 6.3$. Figure 10.31 resulted from (10.70). It is shown that, for a specific layer conductivity $\chi_s = 5$ μS, the critical flashover (withstand) voltage amounts to 105 kV, while for $\chi_s = 50$ μS, the corresponding value is only 49 kV. Model results were compared with experiments reported in the following. At $\chi_s = 10$ μS, the critical flashover voltage U_c, determined by the model, amounts to 83.2 kV, while the measured value is 90.9 kV. At χ_s, = 40 μS, the model value is 52.4 kV while the experimental value is practically identical.

It should be noted, however, that the model is not intended as a substitute for laboratory or field testing. However, the model can be extremely helpful in rationalizing testing and in interpretation of experimental results (Rizk and Rezazada, 1997). It has also proven its validity in establishing the required high-voltage test source capacity for pollution flashover tests (Rizk and Nguyen, 1984, 1988; Rizk and Bourdages, 1985).
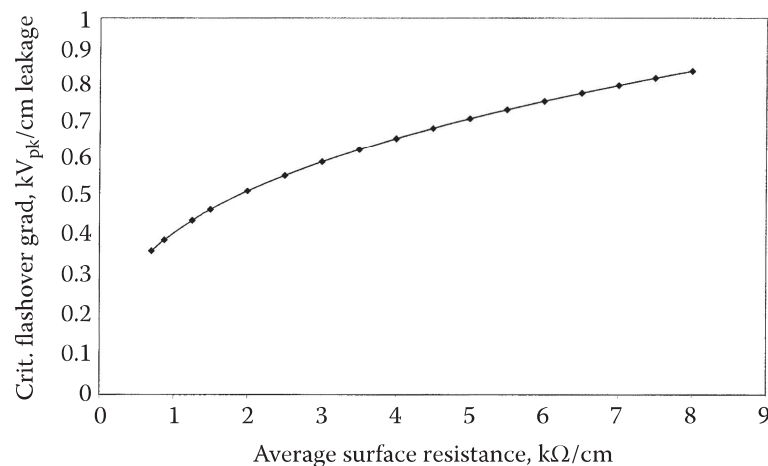

FIGURE 10.30   Variation of critical ac flashover voltage per unit leakage path as a function of average pollution surface resistance per unit leakage path.
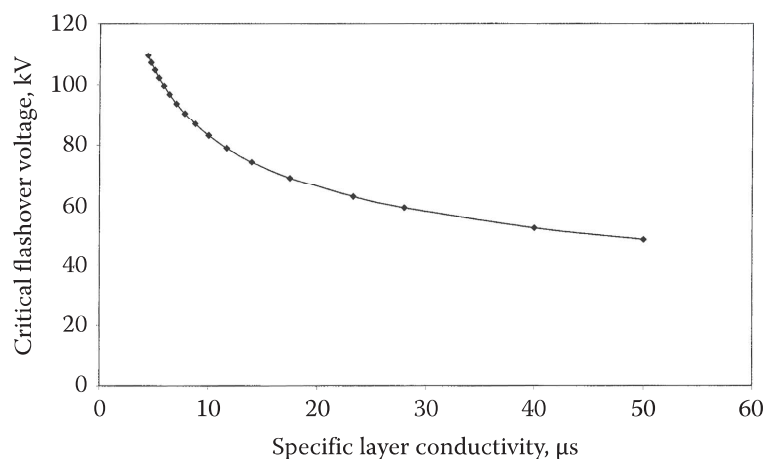

FIGURE 10.31   Variation of critical flashover voltage of long-rod insulator VKL 75/14 with surface layer conductivity as predicted by the Rizk model. $L = 180$ cm; $f = 6.3$.

10.3.3.9.7 Experimental Flashover Characteristics

Pollution flashover test techniques have been specified in IEC 60507 for ac tests (IEC Standards 60507, 1991) and IEC 61245 for dc (IEC Standards 61245, 1993). In the salt fog test, a specified number of nozzles are used to atomize and spray a solution, having a salinity that can be set in the range 2.5–224 kg/m³, towards an energized insulator string. The test can be performed to produce either a withstand voltage or a withstand salinity. This technique produces withstand voltage stresses, kV/m, and order of merit of different insulator designs that appear to be consistent with experience with marine pollution test site results (Lambeth, 1971; Houlgate and Swift, 1990). The solid layer method, on the other hand, produces a pre-deposited pollution layer that is subsequently wetted, often by steam fog. In the clean fog version, wetting occurs under voltage, which is maintained for a specific duration or until flashover occurs. Again, this technique produces either a withstand salt deposit density at a given voltage or a withstand voltage under a given severity. In an earlier version of this test, the so-called kieselguhr method, the voltage is suddenly applied to an already polluted and wetted insulator at maximum specific layer conductivity. This test was intended to simulate the situation of line energization on already polluted and wetted insulators.

Another practical approach is to expose insulators to natural pollution for varying long durations and, subsequently, perform wetting under voltage in the laboratory to determine the withstand voltage (Rizk et al. 1972). This method is certainly more representative of field conditions but is far more time consuming and expensive than artificial pollution tests.

Still another technique is to expose different insulators to natural pollution under voltage and vary the string length to determine the withstand characteristics and order of merit (Lambeth, 1971; Houlgate and Swift, 1990). Again, this is representative of the environment but also very time consuming.

Some typical flashover test results will be presented for insulators A, B, C, D, and E shown in Figure 10.1 with dimensions included in Table 10.1 (Rizk et al. 1972). It should be noted that insulators are usually compared on the basis of their flashover (withstand) characteristics per unit suspension length. This is more relevant to transmission tower design.

Figure 10.32 (Rizk et al. 1972) shows how the different insulator designs are performed in laboratory flashover tests subsequent to field exposure in desert environment for periods extending up to 24 months. It is indicated that, in general, the antifog disc type D had the best flashover voltage per unit suspension length. Although this insulator collected significant pollution due to the deep under ribs, its high ratio of leakage path to spacing (3.05) proved quite favorable. The worst performance was that by type E long-rod VKL 75/14, having the lowest ratio of leakage path/spacing (1.46). It should be noted, however, that
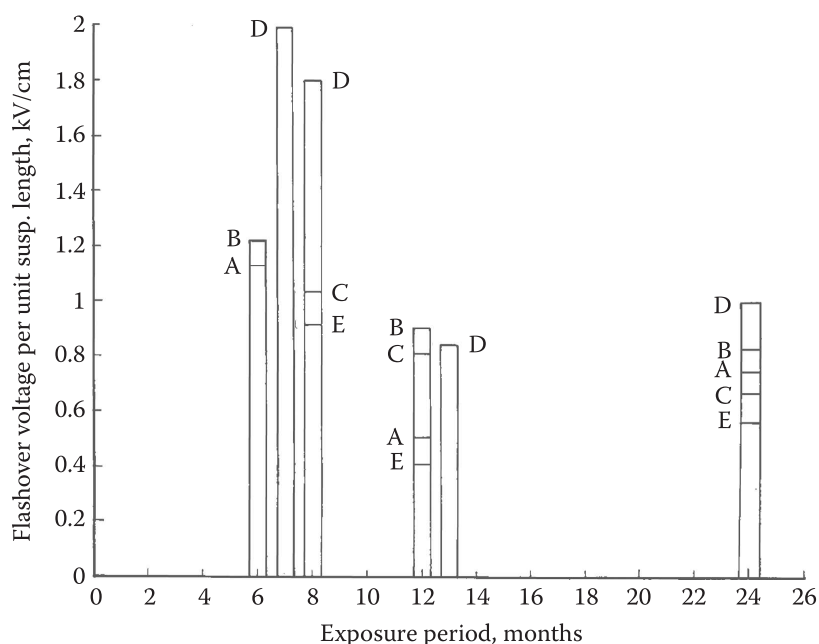

FIGURE 10.32 Flashover voltage per unit suspension length of different insulator designs in laboratory flashover tests subsequent to field exposure in desert environment for periods extending up to 24 months. (From Rizk et al. 1972.)
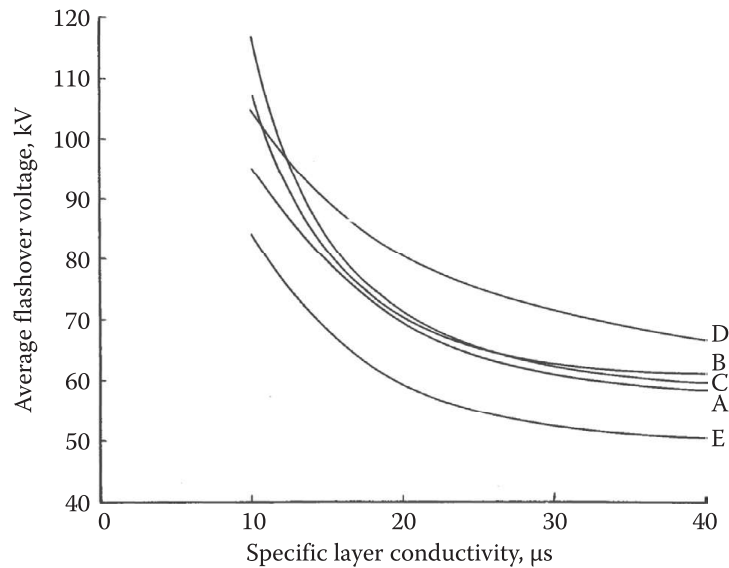
FIGURE 10.33 Variation of average flashover voltage with specific layer conductivity of different insulator strings in a dust deposit test. (From Rizk and El-Sarky, 1972.)

the comparative performance among different insulator designs, in terms of flashover voltage per unit suspension length, was not proportional to the leakage path/suspension length ratio. This is because the critical flashover voltage per unit leakage path length was not the same among different insulator designs exposed to field conditions. For example, after 1-year exposure, the flashover voltage per unit creepage length was 368, 329, 274, and 239 V/cm for insulator types B, C, D, and A, respectively (Rizk et al. 1972). This means that the flat aerodynamic designs B and C had superior critical flashover voltage per unit leakage path, as such designs collect less contaminant in a desert environment.

Figure 10.33 shows variation of the 50% flashover voltage with specific layer conductivity χ_s in the range 10–40 μS for the earlier insulator types in high-voltage dust deposit tests (Rizk et al. 1972). The insulator string length was kept constant at 127 cm ± 6%. Several interesting results were observed. First, artificial tests, at heavy pollution, showed little difference in performance among types B, C, and A, while under field exposure, type B demonstrated clear advantage. Furthermore, the dependence of U_{50} on χ_s can in general for each type, be expressed as

$$U_{50} = \text{const. } c_s^{-b} \tag{10.72}$$

It was found that β amounted to 0.48, 0.40, 0.39, 0.36, and 0.35 for insulator types C, B, A, D, and E, respectively (Rizk et al. 1972).

Salt fog tests according to IEC 60507 were carried out on the same strings. The results are shown in Table 10.7, where the withstand salinities are reported at a test voltage of 63.5 kV $\left(110/\sqrt{3}\ \text{kV}\right)$ and withstand voltages at a salinity of 33.6 g/L. It is observed that the same order of merit is obtained from withstand salinity test as from the U_{50} at constant salinity. The order of merit, however, differs from that

TABLE 10.7

Salt Fog Test Results

String Type	Withstand Salinity at 63.5 kV, g/L	U_{50}, kV at 33.6 g/L Salinity	Order of Merit
A	28	69	3
B	14	60	4
C	40	71	2
D	47.5	86	1
E	7	49	5

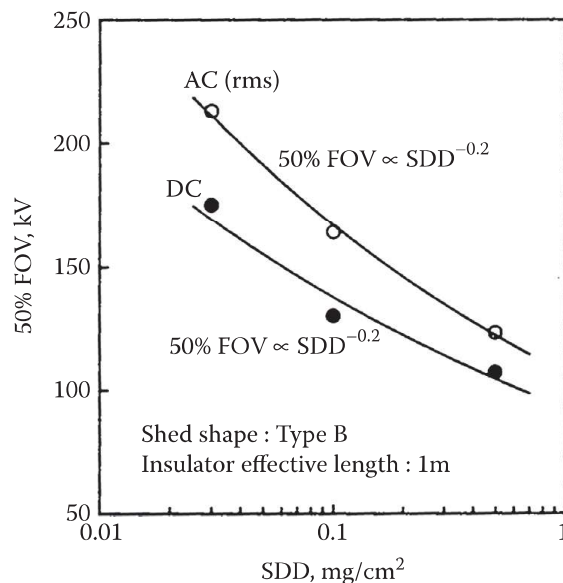*Source:* Rizk et al., CIGRE, Paper No. 33-03, Paris, France, 1972.

FIGURE 10.34 Variation of 50% flashover voltage of silicone rubber insulators with salt deposit density under ac and dc energization. (From Matsuoka, R. et al. Contamination withstand voltage characteristics of polymer insulators, in: *10th ISH*, Vol. 3, Montréal, Québec, Canada, 1997, pp. 81–84.)

obtained from the dust deposit test or from field exposure tests. In particular, the flat aerodynamic disc behaved significantly unfavorably under salt fog.

The aforementioned results confirm that, for transmission line design, insulator selection should be based on a test technique appropriate for the environment.

So far in this section, we dealt with porcelain insulators. It has long been known that polymeric insulators such as silicone rubber, when new, outperform ceramic insulators under pollution. If polymeric insulators completely lose their hydrophobicity, however, they practically behave like ceramic insulators. It has also been known that, in the laboratory, it is difficult to apply and maintain a wet contamination layer on a silicone rubber insulator unless such surface is deliberately deprived from its hydrophobicity in a so-called conditioning process. It is also well known that silicone rubber insulators lose their hydrophobicity, at least temporarily, in service due to surface discharges, sandstorms, heavy rain, and UV radiation (Karady et al., 1994; Rizk et al., 1997). Unless the insulator has seriously aged, hydrophobicity will be recovered in a matter of hours. If exposed to severe pollution and wetting conditions before hydrophobicity is recovered, flashover can take place.

Matsuoka et al. (1997) reported on laboratory contamination tests on different profiles of silicone rubber insulators. It has been shown that insulator performance, for an ESDD = 0.03 mg/cm^2, can be improved by increasing the ratio l/p between the leakage distance l per shed and the shed pitch p up to approximately 4. For a profile with $l = 140$ mm and $p = 50$ mm, Figure 10.34 (Matsuoka et al., 1997) shows the effect of salt deposit density on 50% flashover voltage for both ac and dc energization. It is confirmed that under otherwise the same conditions, dc stress is significantly more severe than ac, as predicted by the earlier model work. It is also shown that, for these unaged polymeric insulators and for the extreme severity of 0.5 mg/cm^2, the 50% flashover stress amounts to approximately 110 kV/m for dc and 125 kV$_{rms}$/m for dc. If comparison is made on the basis of peak voltage, this shows that the ac 50% flashover voltage is 60% higher than dc for the polymeric insulator in question. For a severity of 0.03 mg/cm^2, the ac peak flashover voltage is almost 90% higher than the dc.

10.3.4 Mechanical Requirements

As mentioned in the introduction to this chapter, the importance of mechanical integrity of the line insulators cannot be overemphasized. It should be quite clear that a mechanical failure of the string could lead to conductor dropping and long period out of service. Certainly, this is far more serious than a flashover that can be dealt with by system protection.

In general, the insulator will be subjected to a vertical force F_v due to the conductor weight plus any ice load. A horizontal wind force F_w will also be vectorially added, leading to a resultant force F_r. The vertical load F_v, N could be expressed as

$$F_v = (M_c + M_i) \, g \tag{10.73}$$

where

M_c is the conductor mass for a weight span L_m
M_i is the mass of the ice accumulated
g is the acceleration of gravity

The wind force can be obtained from the design wind speed v_s, which is related to the basic wind speed v_w by (Bayless, 1999)

$$v_s = f_1 \, f_2 \, v_w \tag{10.74}$$

where

f_1 is a topology factor
f_2 is a ground roughness factor

The dynamic pressure q, N/m^2 is obtained from

$$q = k_p v_s^2 \tag{10.75}$$

with $k_p = 0.613$, using SI units (Bayless, 1999).

The wind force F_w can be expressed as

$$F_w = C_f \, q \, A_e \tag{10.76}$$

where

C_f is a force coefficient that depends on conductor shape
A_e is the exposed conductor area for a wind span, with due consideration to possible ice accretion

The resultant force F_r is then given by

$$F_r = \sqrt{F_v^2 + F_w^2} \tag{10.77}$$

For a cap and pin insulator, the electromechanical failing load EMFL is defined as the maximum tensile force reached prior to breakage of the insulator or hardware. Statistically, this is taken as the 50% level minus 3 standard deviations. EMFL is then related to the resultant force F_r by a factor of safety K_s:

$$EMFL = K_s \, F_r \tag{10.78}$$

The safety factor K_s is usually defined for a set of stringing conditions. Examples are as follows:

- $K_s = 5$ at 20° without wind or ice. This means that the everyday working load is 20% of the electromechanical failing load.
- $K_s = 2.5$ at −20°C without wind or ice.
- $K_s = 2.5$ at −5°C with specified wind pressure and ice accretion.
- $K_s = 2.5$ at 5°C at a more severe wind pressure but obviously no ice.

Application to nonceramic insulators is made more complex by the fact that mechanical strength is not a constant but decreases with time due to creep of the core materials (IEC Standard 60815, 2008; Vosloo et al., 2002). In the IEC Standard 60815 (2008), the strength of a polymeric rod is presented as a decaying linear function of the logarithm of the load duration, in minutes. It requires that the slope of

the straight-line relationship be less than 8% of the 1 min failing load per decade of time (a factor of 10). The IEC strength curve $F(t)$ can be expressed as

$$F(t) = F(1) - 0.08 \log_{10}(t)$$ (10.79)

where

$F(t)$ is the residual strength after a duration t

$F(1)$ is the 1 min strength, which means that after 50 years of service, the residual mechanical strength should be above approximately 40% of the initial 1 min strength

It was argued in Vosloo et al. (2004), however, that actual tests show that after such period, about 65% of the original 1 min strength is retained. Obviously, laboratory test results were substantially extrapolated to 50 years (de Tourreil et al., 1985).

The 1 min strength specified by the manufacturer is referred to as the *specified mechanical load*, SML, of the polymeric insulator. Similar to the case of ceramic insulators, here, SML is related to the resultant force F_r by

$$SML = K_s \cdot F_r$$ (10.80)

where, as mentioned earlier, K_s is the factor of safety.

Standard IEEE cap and pin insulators (5′(3/4)/10′/or 146/254 mm) are commercially available with electromechanical ratings of 70–160 kN (15,000–36,000 lb). Antifog discs are available for up to 530 kN (120,000 lb). Silicone rubber long-rod insulators are also available for SML ratings of 110–350 kN (25,000–80,000 lb).

10.4 Insulator Selection

10.4.1 Insulator Type and Material

The selection of transmission line insulators includes the determination of the type, material, and insulator characteristics. Reference should be made to treatment of these aspects earlier in this chapter and elsewhere. A summary is included in the following.

The first decision is regarding the use of ceramic or polymeric insulators (Papaliou and Schmuck, 2013). The following are reiterated:

- Polymeric insulators have favorable mechanical strength to weight ratio. However, deterioration of failing mechanical load over the insulator lifetime must be considered.
- Polymeric insulators are less vulnerable to vandalism.
- Polymeric insulators have favorable pollution performance when new. However, they are exposed to occasional loss and recovery of hydrophobicity. The designer has to consider suitability of such insulators to the particular environment.
- Ultimately, under aging factors, nonceramic insulators are bound to lose their hydrophobicity as the LMW silicon oil that diffuses to the surface and is responsible for hydrophobicity will be practically depleted. The designer has therefore to decide whether to take advantage of the superior performance of nonceramics when new and accept replacement at an earlier time. The other choice, which may be more prudent, is to use the same design stress as for porcelain or glass.
- Also, consideration must be given to the effect of aging not only on electrical characteristics but also on mechanical integrity, which may dictate a shorter lifetime compared to porcelain or glass.
- At system voltage of 245 kV and above, special care must be given to the design of corona rings in order to inhibit surface discharges that would otherwise accelerate aging of the polymeric insulator.
- The user has to be aware that application of polymeric insulators requires a follow-up in service that is more demanding than would be the case for porcelain (puncture) or glass (shattering).

If the decision is made to use conventional ceramic insulators, the designer has to choose between porcelain and glass. As mentioned earlier in this chapter,

- In high-voltage laboratory, pollution tests porcelain and glass insulator performance is practically identical
- In service, glass insulators may be more vulnerable to surface cracks induced by erosion due to severe flow of leakage current in polluted environment
- In service, the detection of punctured porcelain units requires specialized techniques, while shattering of glass units is easily identified

The earlier arguments apply for new designs of conventional transmission lines. For compact line design or for mechanical or electrical upgrading of operating lines, the lack of air clearances and the necessity of supporting heavier conductor bundles may favor the application of polymeric insulators (Papaliou and Schmuck, 2013).

10.4.2 Insulator Profile

The IEC Standard 60815 (2008) defines four levels of pollution: I, light; II, medium; III, heavy; and IV, very heavy, with minimum nominal specific creepage distance of 16, 20, 25, and 31 mm/kV$_{LL}$, respectively. When referred to phase-to-ground voltage, the specific leakage distances become 28, 35, 43, and 54 mm/kV, respectively. Several parameters are given to characterize the insulator or a complete string:

- The minimum distance between sheds
- The ratio between spacing and shed overhang
- The local, as distinct from overall, ratio between creepage distance and clearance
- Alternating sheds
- Inclination of sheds
- Two parameters characterizing the entire insulator (string):

  1. Creepage factor (CF): defined as the ratio between the total leakage distance and the arcing distance
  2. Profile factor (PF): defined as the ratio between the so-called *simplified* and real leakage path between consecutive sheds and insulator units

For reference to detailed drawings, please refer to the IEC Standard 60815 (2008).

Some recommendations are given concerning the limits of the aforementioned parameters. For example, it is advised to keep CF $\leq$ 3.5 for pollution levels I and II and CF $\leq$ 4.0 for pollution levels III and IV. Experience has shown that increasing CF beyond these limits is not effective in improving insulator performance.

The standard (IEC Standard 60815, 2008) recognizes, as can be deduced from the earlier model, that pollution performance can deteriorate for insulators with large average diameter (lower r_p for the same χ_s or ESDD). For a mean diameter d_m below 300 mm, no increase of the specific leakage path is recommended. However, for $300 \leq d_m \leq 500$ mm, a 10% increase in the specific leakage path is recommended. For $d_m > 500$ mm, a 20% reinforcement of the specific leakage path is recommended.

It is considered that, while IEC 60815 (IEC Standard 60815, 2008) contains useful general classifications and recommendations, it is by no means adequate for insulator selection in polluted environment. The subject will be treated in more depth in the following.

10.4.3 Design Approach

10.4.3.1 Flowchart

Figure 10.35 shows a proposed flow chart (Rizk, 1997) for the selection of high-voltage insulators in polluted environment. The chart will be briefly explained in this section, but details of the different stages in the selection process will be dealt with in later sections.
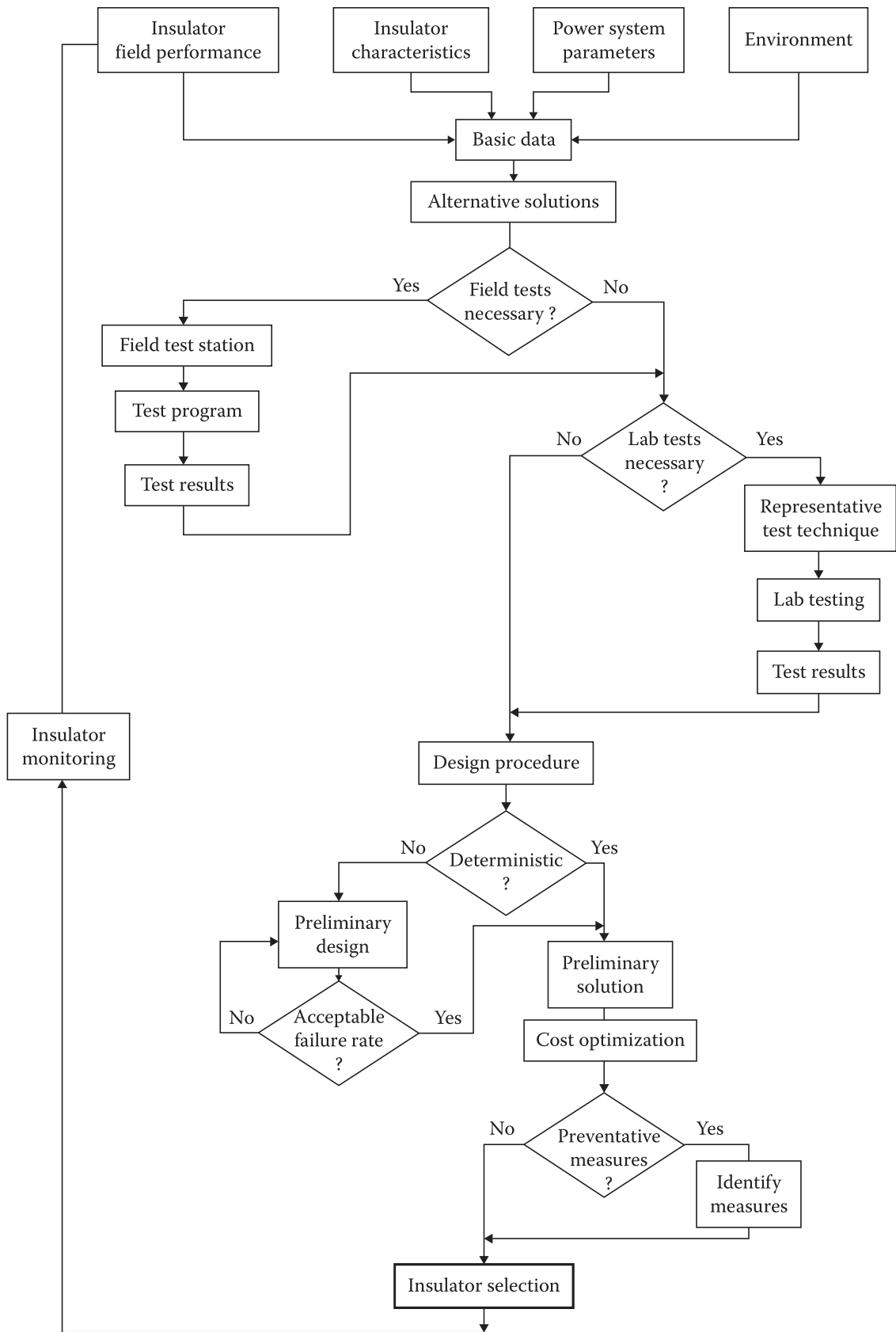
FIGURE 10.35 Flow chart for insulator selection in polluted environment.

The chart starts with the basic data available to the design engineer related to relevant power system parameters: ac or dc, line voltage, frequency, transmission line length, level of overvoltages, environmental parameters (type of environment, pollutants, rain, wind, fog, dew, etc.), as well as any available information on insulator type, designs, and pollution performance both from the field and in the laboratory. At this stage, some alternative solutions could be envisaged, for example, different profiles of porcelain cap and pin insulators and different designs of silicone rubber rods. A decision has to be made early on whether field tests on the selected alternative designs would be necessary. That decision should be based on adequacy of field and laboratory results on the performance of the alternative designs in the specific or similar environment to that of the proposed route. It is essential to reach the decision on field tests early, since field tests would normally require 2–4 years. If such time is not available, the decision is simple: no meaningful field testing program could be undertaken. Otherwise, a field test station has to be designed and a test program prepared and implemented.

The other question that has to be settled as early as possible is that of the necessity of high-voltage pollution tests in a laboratory. Again, this will be based on the adequacy of available material on the performance of the different insulators considered. If the decision is taken to test, a test most representative of the environment concerned has to be selected. It could suitably be one of the standard tests of salt fog or clean fog or some modified variance thereof.

In the design procedure, a decision has to be made on whether to follow a deterministic approach, in which a safety margin between the operating voltage and the withstand voltage of the polluted string is adopted, or a statistical approach, in which insulators are selected to meet a predetermined performance criterion. While the statistical approach is more scientifically appealing, it requires more complete information on the environmental *events* and flashover characteristics of polluted insulators as well as a sensible determination of what an *acceptable* failure rate is.

Once the selected insulators are installed, a follow-up of their performance in service will provide necessary information for any remedial or maintenance procedures needed as well as input for selection of insulators for future lines and installations.

10.4.3.2 Statistical Approach to Insulator Selection

It is well known that, for a given pollution severity expressed by equivalent deposit density ESDD, specific layer conductivity χ_s, or mean surface resistance r_p per unit leakage length and adequate wetting, for example, caused by dew formation or light drizzle, the flashover voltage of an insulator string is a statistical variable often described by a normal distribution:

$$P(V) = \phi\left(\frac{V - U_{50}}{s}\right) \tag{10.81}$$

where
  V is the applied voltage
  U_{50} is the 50% flashover voltage
  σ is the standard deviation, all expressed in kV
  ϕ is the cumulative normal distribution function

In dealing with many strings in service and considering that, for adequately insulated lines, we are facing low-probability situations, it is important to realize that for physical reasons, flashover cannot occur below a certain threshold voltage U_o, which can be related to U_{50} by

$$U_o = U_{50} - n\sigma \tag{10.82}$$

where n is a number usually assumed as 2, 3, or 4. This means that instead of (10.81), we should have

$$P(V) = \frac{\left[\phi\left(\frac{V - U_{50}}{s}\right) - \phi(-n)\right]}{1 - \phi(-n)} \tag{10.83}$$

The truncation will obviously influence the low-probability region only and (10.81) will still be practically valid at higher probabilities. In the earlier equations, U_{50} and σ, which usually is proportional to U_{50}, are functions of pollution severity.

Another statistical distribution, the Weibull distribution, has the built-in truncation property mentioned earlier and, moreover, provides a simple manipulation when dealing with multiple stressed objects assumed to act as independent statistical variables. Instead of (10.81), we may then have

$$P(V) = 1 - \exp\left[-\left(\frac{(V - U_o)}{bU_o} \right)^k \right] \tag{10.84}$$

where U_o, β, and k are the Weibull distribution parameters and U_o is determined from (10.82), once n has been selected.

Since most available high-voltage test results are expressed in terms of the normal distribution, it is required to determine the equivalent Weibull distribution. The parameters β and k can then be determined if we impose two conditions of equivalence. In reference (IEC Standard 60071-2, 1996), these two conditions require that the two distribution functions have the same values so that $P(V) = 0.5$ at $V = U_{50}$ and $P(V) = 0.16$ at $V = U_{50} - \sigma$.

These constraints result in the following formulae:

$$k = \frac{1.38}{\ln\left(n/(n-1)\right)} \tag{10.85}$$

and

$$b = \frac{n \cdot c}{(1 - n \cdot c)(\ln 2)^{1/k}} \tag{10.86}$$

where the coefficient of variation $c = \sigma/U_{50}$ is obtained from the normal distribution. Table 10.8 shows the values of k for different values of n.

As numerical examples, for $c = 0.10$ and $n = 2$, (10.86) yields $\beta = 0.30$, while for $c = 0.08$ and $n = 3$, β is determined at 0.352.

For a number of strings N stressed simultaneously and assumed statistically independent, the probability of flashover becomes

$$P_N(V) = 1 - \exp\left[-N\left(\frac{V - U_o}{bU_o} \right)^k \right] \tag{10.87}$$

which, for $NP \ll 1$, yields

$$P_N(V) \cong N\left(\frac{V - U_o}{bU_o} \right)^k \tag{10.88}$$

Dividing the applied voltage V and the withstand voltage U_o by the string length to obtain E and E_o, respectively, (10.88) when referred to one string becomes

$$P_N(V) \cong \left(\frac{E - E_o}{bE_o} \right)^k = \text{const.}\left(\frac{E - E_o}{E_o} \right)^k \tag{10.89}$$

where the constant amounts to $(1/\beta)^k$.

TABLE 10.8

Exponent k of the Equivalent
Weibull Distribution

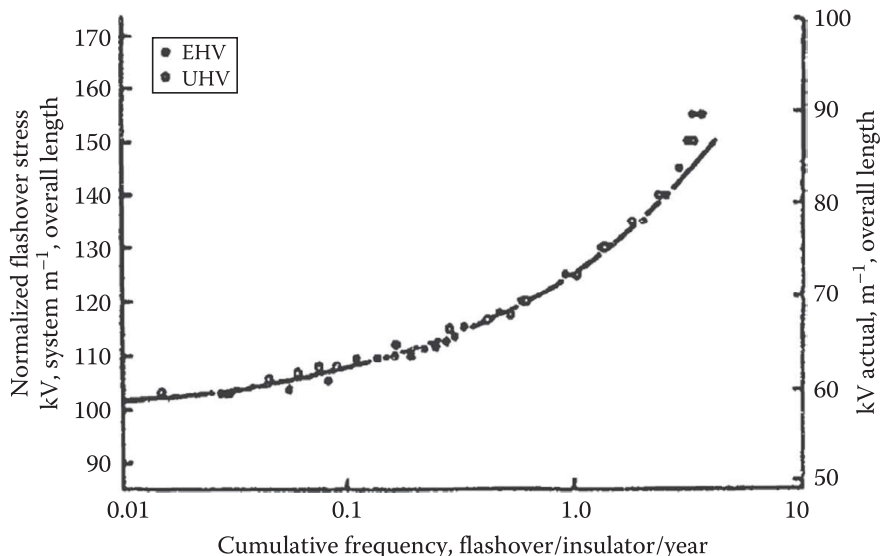| n	2	3	4
k	2.0	3.4	4.8

FIGURE 10.36 Cumulative flashover distribution of an insulator string in marine environment. (From Houlgate, R.G. et al., The performance of insulators at extra and ultra high voltage in a coastal environment, CIGRE, Paper 33-01, 1982.)

Figure 10.36 shows cumulative flashover distribution curve, referred to one string, of insulator exposed to marine pollution at the Brighton test station (Houlgate et al., 1982). The results fit expression (10.89) with $E_o = 99$ kV/m (referred to system voltage, actual stress $E_o = 99/\sqrt{2}$ kV/m) and $k = 2.1$, which from Table 10.8 corresponds to $n = 2$ (Houlgate et al., 1982).

Having shown that field experience substantiates the statistical approach developed so far on the basis of a Weibull distribution, we will extend the approach to predict line performance.

The information needed for such an approach comprise the variation of pollution severity along the line route as well as the frequency of dangerous wettings (Rizk et al., 1975) constituting the statistical events. Figure 10.37 shows the variation of ESDD on three types of insulators during 32 months exposure at Ghazlan, Saudi Arabia (Akbar and Zedan, 1991). SPI is a standard porcelain, FP1 is antifog
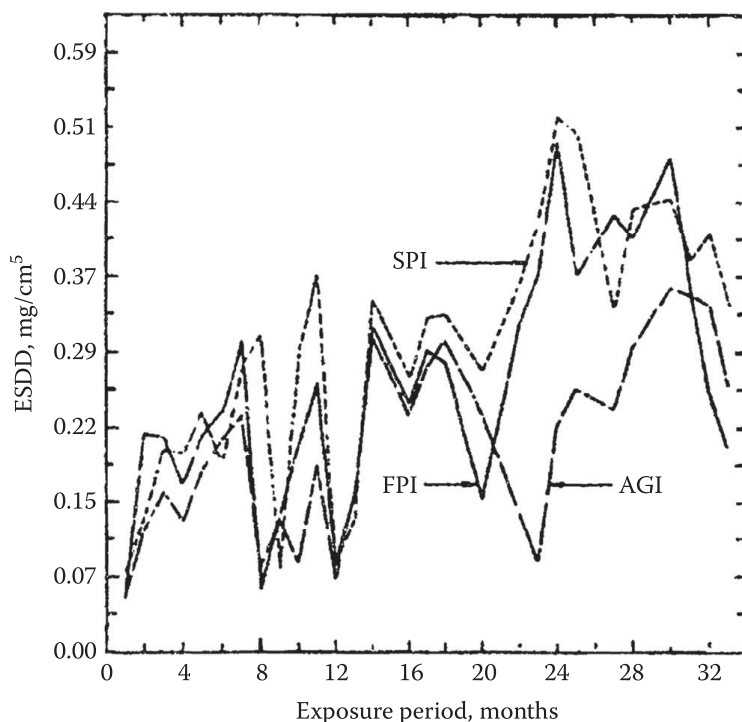

FIGURE 10.37 Variation of ESDD with exposure period for different insulators in desert environment. (From Akbar, M. and Zedan, F.M.., *IEEE Trans. Power Deliv.*, 6(1), 429, January 1991.)
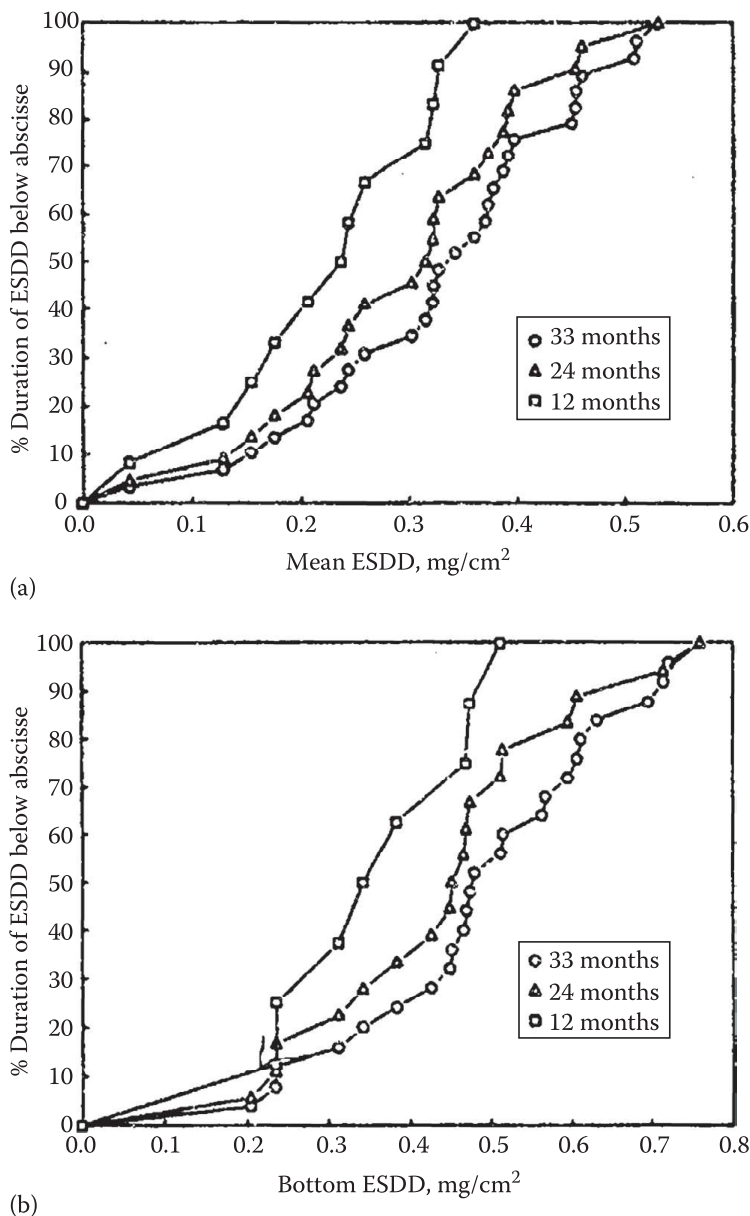
(a)

(b)

FIGURE 10.38 Cumulative severity–duration curves for different insulators in desert environment. (From Akbar, M. and Zedan, F.M.., *IEEE Trans. Power Deliv.*, 6(1), 429, January 1991.)

porcelain, and AG1 is aerodynamic glass insulators. It is once more confirmed that severity varies with the insulator profile (Figure 10.37).

It was suggested by Rizk that severity measurements could be more readily interpreted if presented as severity–duration curves as shown in Figure 10.38. It is shown that the difference between the 24 and 33 months curves is much less significant than between the 12 and 24 months characteristics, confirming that a minimum exposure period of 2–3 years is needed for meaningful results in this environment. It is also evident that the 50% severity values are more stable than the extreme ESDD values.

Let us consider a section of a high-voltage transmission line where both pollution severity and wetting conditions could be considered reasonably uniform. Let the number of strings in this section be N_i. Also, divide the exposure period T into subintervals ΔT_v, so that within such subinterval, the pollution severity does not vary significantly and the number of dangerous wetting events be w_{iv}. From (10.87), the number of flashovers in this section within this time subinterval will be

$$n_{\text{fiv}} = w_{\text{iv}} \left\{ 1 - \exp\left[-N_i \left(\frac{V - U_{\text{oiv}}}{b U_{\text{oiv}}} \right)^k \right] \right\}$$

(10.90)

which, if the condition leading to (10.88) is satisfied, becomes

$$n_{\mathrm{fiv}} \cong w_{\mathrm{iv}} N_i \sum_1 \left[\frac{(V - U_{\mathrm{oiv}})}{b U_{\mathrm{oiv}}} \right]^k \qquad (10.91)$$

Here, the letter i refers to the section and v to the subinterval, so that n_{fiv} is the number of flashovers in section i during subinterval v and U_{oiv} is the corresponding withstand voltage. Over the whole exposure period considered, the total number of flashovers n_{f} is obtained by a double summation overtime and line sections:

$$n_{\mathrm{f}} = \sum_i \sum_v w_{\mathrm{iv}} N_i \sum_1 \left[\frac{(V - U_{\mathrm{oiv}})}{(b U_{\mathrm{oiv}})} \right]^k \qquad (10.92)$$

As mentioned earlier, this could be expressed in terms of the applied and withstand gradients E and E_{oiv}:

$$n_{\mathrm{f}} = \sum_i \sum_v w_{\mathrm{iv}} N_i \sum_1 \left[\frac{E - E_{\mathrm{oiv}}}{b E_{\mathrm{oiv}}} \right]^k \qquad (10.93)$$

This equation represents a dynamic statistical model of line performance since both E_{oiv} and w_{iv} are functions of time.

For any section or subsection of the line, the specific number of faults can be introduced as the number of faults per string per wetting event, that is, $n_{\mathrm{f}}/(w \cdot N)$.

For any time subinterval, from (10.91), this could be expressed as

$$\frac{n_{\mathrm{f}}}{(w \cdot N)} \cong \sum_1 \left[\frac{E - E_{\mathrm{o}}}{b E_{\mathrm{o}}} \right]^k \qquad (10.94)$$

As an example, consider a 60 km section of a 525 kV transmission line. The nominal span is 400 m, so that the number of strings per section $N = 450$. The number of dangerous wettings per year is given as $w = 10$. The type of insulator tested at the relevant pollution severity showed a 50% flashover gradient $E_{50} = 60$ kV/m of suspension length. Based on experience, the distribution parameters were taken as $n = 3$ and $c = 0.08$. The earlier expressions resulted in $E_{\mathrm{o}} = 45.6$ kV/m and the Weibull distribution parameter $\beta = 0.35$. The performance criterion of 1F/100 km · year results in $n_{\mathrm{f}} = 0.6$ faults/year for the 60 km section.

From (10.94), the operating voltage gradient is determined at $E = 47.0$ kV/m, which, from the operating phase-to-ground voltage of 303 kV, results in a design suspension string length of 6.46 m. The cap and pin insulator in question had a unit spacing of 170 mm, so that the number of string units required becomes 38.

REFERENCES

Adamson, A.W. *Physical Chemistry of Surfaces*, 2nd edn. New York: Wiley-Interscience, 1967, Chapter 7.

Akbar, M., Ahmed, Z., Matsuoka, R., Sakanishi, K., and N. Okada. Insulation contamination study in Pakistan (Part I). In: *9th ISH*, Graz, Austria, 1995, Paper 3208.

Akbar, M. and F.M. Zedan. Performance of HV transmission line insulators in desert conditions. Part III: Pollution measurements at a coastal site in the eastern region of Saudi Arabia. *IEEE Transactions on Power Delivery* 6(1): 429–438, January 1991.

Akbar, M., Zedan, F.M., Abdul-Majeed, M.A., and K.T. Al-Soufi. Design of HV lines to combat insulator pollution problems in the eastern region of Saudi Arabia. *IEEE Transactions on Power Delivery* 6(4): 1912–1921, October 1991.

Bartnikas, R. Dielectrics and insulators. In: R.C. Dorf (ed.), *Electrical Engineering Handbook*. Boca Raton, FL: CRC Press, 1993, Chapter 52.